THE JOURNAL OF PHYSICAL CHEMISTRY B

ARTICLE

pubs.acs.org/JPCB

Understanding Rhodopsin Mutations Linked to the *Retinitis pigmentosa* Disease: a QM/MM and DFT/MRCI Study

Erix Wiliam Hernández-Rodríguez,[†] Elsa Sánchez-García,[*,‡] Rachel Crespo-Otero,[‡] Ana Lilian Montero-Alejo,[§] Luis Alberto Montero,[§] and Walter Thiel[‡]

[†]Departamento de Bioquímica, Instituto de Ciencias Básicas y Preclínicas "Victoria de Girón", 11600 Havana City, Cuba, and Charité Centrum für Innere Medizin und Dermatologie, Biomedizinisches Forschungszentrum, Campus Virchow, Charité-Universitätsmedizin, 13353 Berlin, Germany

[‡]Max-Planck-Institut für Kohlenforschung, Mülheim an der Ruhr, 45470 Germany

[§]Laboratorio de Química Computacional y Teórica, Departamento de Química Física, Universidad de La Habana, 10400 Havana City, Cuba

Supporting Information

ABSTRACT: *Retinitis pigmentosa* (RP) is a pathological condition associated with blindness due to progressive retinal degeneration. RP-linked mutations lead to changes at the retinal binding pocket and in the absorption spectra. Here, we evaluate the geometries, electronic effects, and vertical excitation energies in the dark state of mutated human rhodopsins carrying the abnormal substitutions M207R or S186W at the retinal binding pocket. Two models are used, the solvated protein and the protein in a solvated POPC lipid bilayer. We apply homology modeling, classical molecular dynamics simulations, density functional theory (DFT), and quantum mechanical/molecular mechanical (QM/MM) methods. Our results for the wild type bovine and human rhodopsins, used as a reference, are in good agreement with experiment. For the mutants, we find less twisted QM/MM ground-state chromophore geometries around the $C_{11}-C_{12}$ double bond and substantial blue shifts in the lowest vertical DFT excitation energies. An analysis of the QM energies shows that the chromophore−counterion region is less stable in the mutants compared to the wild type, consistent with recent protein folding studies. The influence of the mutations near the chromophore is discussed in detail to gain more insight into the properties of these mutants. The spectral tuning is mainly associated with counterion effects and structural features of the retinal chain in the case of the hM207R mutant, and with the presence of a neutral chromophore with deprotonated Lys296 in the case of the hS186W mutant.

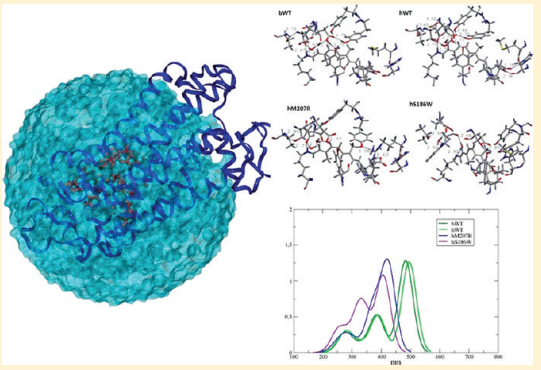

INTRODUCTION

Retinitis pigmentosa (RP), a condition associated with blindness,[1] is related to progressive retinal degeneration caused by the death of the vertebrate photoreceptors dedicated to dim light vision (rod photoreceptor cells).[2,3] Rhodopsin is the visual pigment in rods and a heptahelical transmembrane receptor protein expressed in retina.[4,5] It is composed of four building blocks: (a) an apoprotein opsin with 348 amino acid residues, (b) a covalently bound chromophore (retinal), (c) two palmitoyl residues linked to Cys322 and Cys323, and (d) two sugars linked to Asn2 and Asn15.[6] In the dark state, the chromophore is 11-*cis*-retinal, which forms a retinal protonated Schiff base (RPSB) linkage with Lys296 at the rhodopsin binding pocket (RBP) (Figure 1).

Visible light absorption at ∼500 nm[7] by the pigment triggers the isomerization of the 11-*cis* form of the RPSB to the nonprotonated *all-trans* form of the retinal Schiff base linked to the opsin.[6,8] This reaction occurs with high efficiency (quantum yield of 0.65−0.67)[8,9] and provides rhodopsin with the energy to form the active state.[10,11] The primary photoproduct, photorhodopsin (photo), is generated within a very short time (200 fs) and thermally relaxes within a few picoseconds to a distorted *all-trans* configuration, bathorhodopsin (batho), which is in equilibrium with a blue-shifted intermediate (BSI) before forming lumirhodopsin (lumi). Metarhodopsin I (meta I) is the next intermediate followed by metarhodopsin II (meta II), the active conformation for G-protein coupling.[6] The meta II state is formed by translocation of the Schiff base proton to Glu113, which plays the role of counterion for the RPSB in the dark state.[8,9] This sequence of events results in the excitation of the visual nerve and the perception of light in the brain.[12] Meta II

Received: April 21, 2011
Revised: October 14, 2011
Published: November 29, 2011

ACS Publications © 2011 American Chemical Society

dx.doi.org/10.1021/jp2037334 | *J. Phys. Chem. B* 2012, 116, 1060–1076

decays to metarhodopsin III (meta III) and later to opsin and free 11-*trans*-retinal (Scheme 1).[6]

Many experimental and computational studies are available for bovine rhodopsin (bWT).[9,10,12−19] However, much less work has been reported for human rhodopsin (hWT) whose crystal structure is not yet available.[20−23]

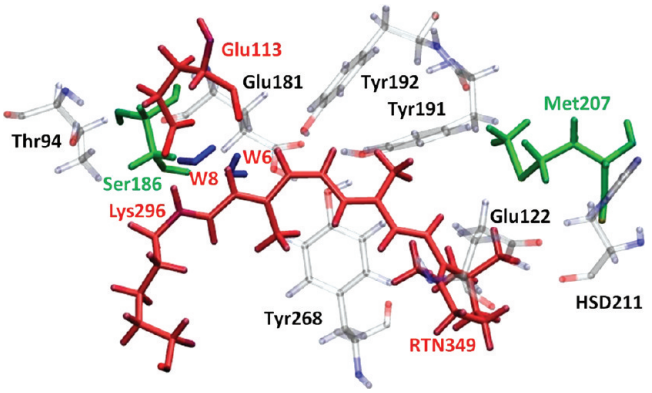

Figure 1. Rhodopsin binding pocket from one snapshot of the human wild type rhodopsin. The QM region is shown in red (water molecules in blue) and the residues to be mutated in green. The notation for the residues is the same as in the pdb file 1U19.

Mutations affecting rhodopsin can lead to loss of the outer field of vision.[24] Over 120 point mutations have been discovered in the rhodopsin gene. Patients suffering from *Retinitis pigmentosa* caused by rhodopsin mutations display night blindness as well as progressive loss of peripheral and, eventually, central vision.[3,24−27] Some mutation mechanisms are still unclear, and no definitive treatment is available today.

Mutations associated with *Retinitis pigmentosa* can cause an impairment of protein folding or expression or retinal binding[28−30] and thus affect rhodopsin function. Some of these processes could be influenced by drug intake.[23] Understanding the effects of mutations on light absorption and photoisomerization may thus be relevant for medical purposes.

Extensive mutagenesis studies on rhodopsin have established the role of key residues. For example, replacement of Pro267 has consequences for opsin folding, membrane insertion, assembly, and/or function.[31] RP-associated mutation experiments for cysteines in rhodopsin show that the disulfide bond between Cys110 and Cys187 is necessary for an appropriate folding and receptor function.[32,33] Trp265 mutations have a large effect on the spectral properties of rhodopsin, changing the retinal binding site.[31] Substitutions at Phe261 and Gly121 affect the early steps of the

Scheme 1. Rhodopsin Photocycle[6 a]

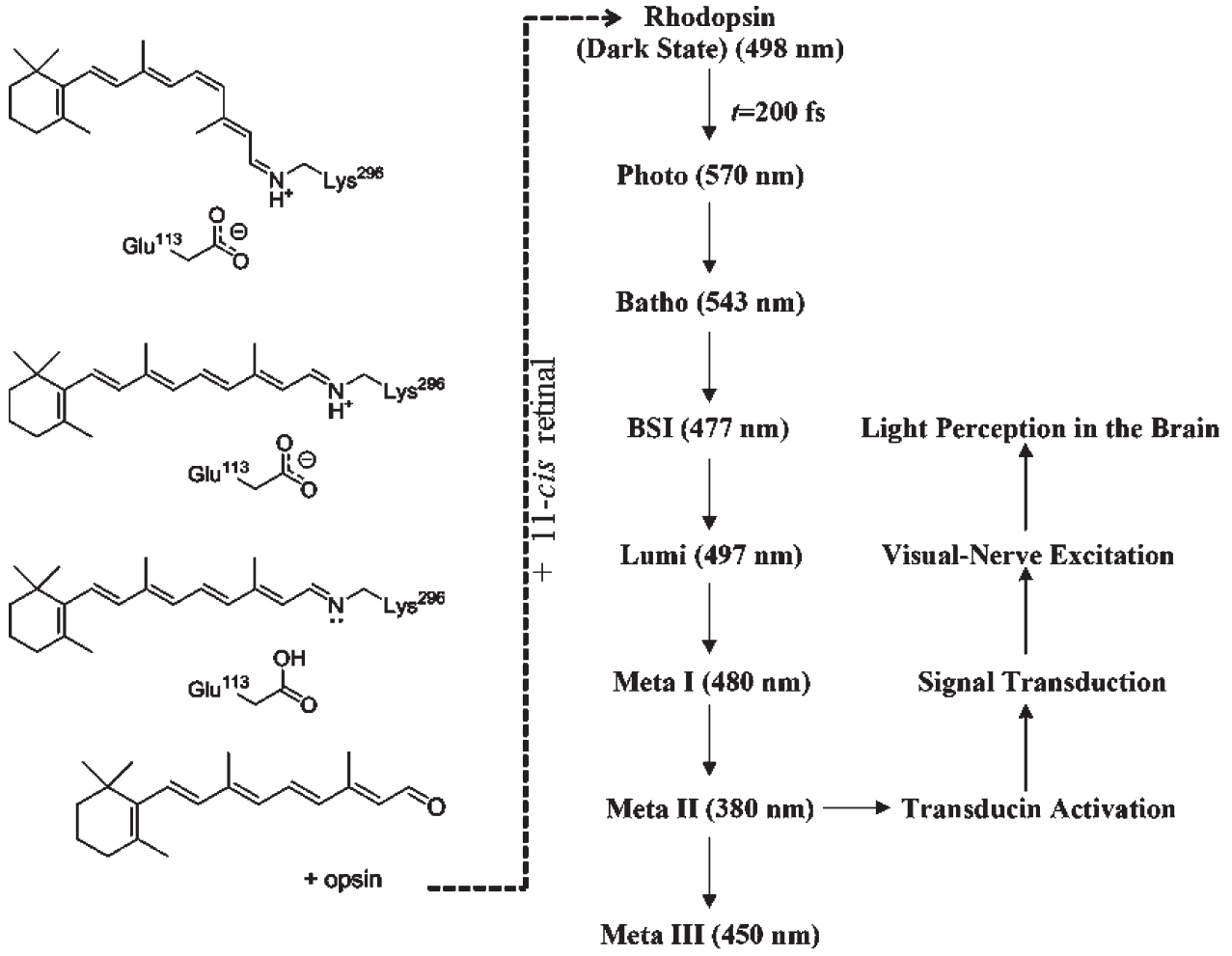

[a] The λ_{max} values are shown in parentheses.

dx.doi.org/10.1021/jp2037334 |J. Phys. Chem. B 2012, 116, 1060–1076

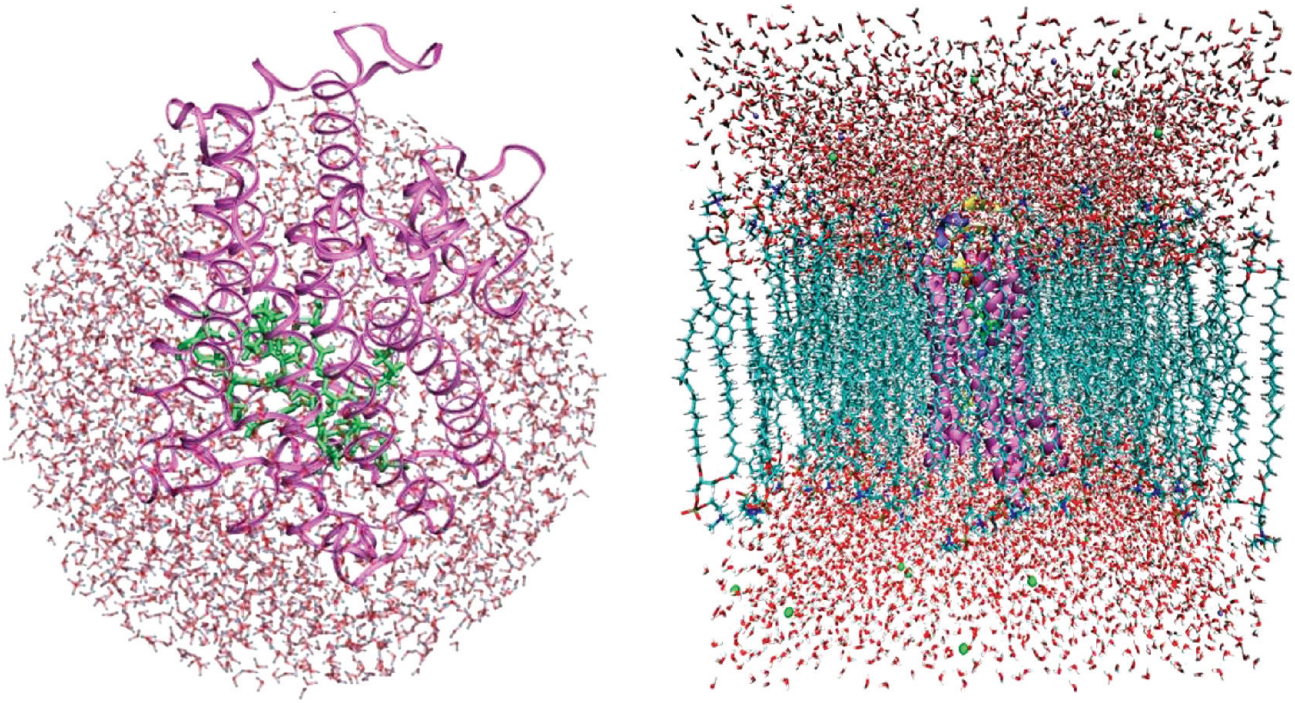

Figure 2. Solvated rhodopsin (left, model I) and the rhodopsin/membrane/water/ion complex (right, model II).

photoisomerization, producing blue-shifted intermediates.[34] In vitro studies using recombinant rhodopsin with amino acid substitutions associated with RP in different positions of the rhodopsin structure, including the RBP, show a modified spectral behavior.[22,28] Several other mutants have also been investigated, including E113Q, E181Q, G90D, A292S, A269T, H211C, and D83N, which display diverse light absorption patterns.[12,14]

The M207R and S186W mutations affect the RBP and cause the autosomal dominant form (ADRP) of RP.[28] A recent experimental study[35] reports that the mutation M207R allows for rhodopsin folding and rhodopsin regeneration with 11-*cis*-retinal, increasing the experimentally observed concentration of the chromophore. Light absorption has been detected in the dark state, outlining possible changes of the protonation state for the Schiff base linkage (SBL).[35] A low misfolding at the second extracellular loop has been reported for the mutation S186W.[36] This mutation thermally destabilizes rhodopsin and increases the rate of thermal isomerization.[37] An exploratory but limited theoretical study of the M207R and S186W mutations has been previously performed by some authors of this paper.[38] Very recently, a computational study by Rakoczy et al. using FoldX analysis on disease-linked rhodopsin mutations included M207R and S186W.[23] They classified the mutations according to their effect on the stability of the protein and found that both substitutions cause some destabilization.[23] However, despite their importance for the development of prospective therapies, to the best of our knowledge, there have not yet been reported any detailed theoretical studies of the M207R and S186W mutations at the molecular level.

It is known that the optical properties of the chromophores in retinal proteins are modulated by the protein environment. Three general mechanisms are commonly considered for the spectral tuning: distortion of the retinal geometry due to steric interactions with the protein binding pocket, interaction of the RPSB with the counterion Glu113 balancing its positive charge, and interactions of the retinal with the polar amino acid residues lining the binding pocket.[39−45]

Both substituted residues (207 and 186) extend into the RBP (Figure 1) and are near the chromophore in the three-dimensional (3D) rhodopsin structure. Therefore, the M207R and S186W mutations may induce structural changes that affect the dark state geometry of the RBP, and/or electronic perturbations that impair the mechanisms of spectral tuning and/or photoisomerization.

Here, we use homology modeling[46] combined with classical molecular mechanics (MM) optimizations and molecular dynamics (MD)[47] to generate a 3D structure of hWT from bWT. The mechanisms of RP-associated mutations affecting the RBP in human rhodopsin are investigated in the biological environment by means of MD simulations[47] and QM/MM[48] geometry optimizations using DFT methods for the QM region. Vertical excitation energies are calculated by a DFT-based multireference configuration interaction (DFT/MRCI) treatment[49] and time-dependent TDDFT methods.[50−53] Two models are used (Figure 2), the protein in a water sphere (model I) and the protein in a solvated POPC lipid bilayer (model II), to evaluate the effect of the M207R and S186W mutations on the retinal structure and the absorption spectra. We analyze the effect of these mutations and discuss their possible consequences regarding photoisomerization and potentially harmful side reactions.

■ COMPUTATIONAL DETAILS

Starting Structure. Our models are based on the 2.2 Å X-ray structure of bovine rhodopsin (Protein Data Bank code: 1U19).[14,54] They contain protein chain B including opsin, 11-*cis*-retinal and two palmitic acid residues linked to Cys322 and Cys323, as well as 29 crystal water molecules in chain B. Omitted were metal ions and other non-amino acid residues as well as the sugar residues linked to Asn2 and Asn15, which do not significantly influence the protein dark state properties in experimental studies.[29]

Homology Modeling. 3D models were generated by homology modeling techniques using the bovine rhodopsin structure as a template as described above. This was done for human-WT rhodopsin (hWT), the human-M207R mutant (hM207R), and the human-S186W mutant (hS186W). For the sake of consistency, the same technique was also applied to build models for bovine-WT rhodopsin (bWT), even though the starting geometry comes from bWT.

The data to build the M207R and S186W mutations was collected from the International *Retinitis Pigmentosa* Association (IRPA) databases.[28] The homologous proteins were identified using BLAST (Basic Local Alignment Search Tool).[55] The rhodopsin sequences, obtained from the TrEMBL and SWISS-PROT databases of the ExPASy Molecular Biology Server,[56] reached a significant BLAST score of 93% with the crystal structure of bovine rhodopsin, 1U19.[14] Homology models were built using MODELLER in version 9v7,[57] the Cys110−Cys187 disulfide bridge was successfully generated in all structures, and the 29 crystal waters and the palmitoyl moieties connected to Cys322 and Cys323 in bWT were conserved. Five models with all hydrogen atoms included were calculated for each system. The positions of the internal water molecules, including two of them near the chromophore in the RBP, are in excellent agreement with the resolved water binding sites in the crystal structure for the WT models, and are as expected for the mutants. The models were optimized by the variable target function method (VTFM, normal schedule) using the conjugated gradient (CG) algorithm and refined using MD (fast level) with simulated annealing (SA).[57,58] The DOPE-HR method was employed for selecting the model with the lowest discrete optimized protein energy (DOPE) using the standard MODELLER energy function.[57]

pK_a Calculations. pK_a values were calculated for all titratable amino acid residues in the structures bWT, hWT, hM207R, and hS186W with all non-hydrogen atoms, both in the protein and in the ligands (11-*cis*-retinal, palmitoyl moieties, and waters) using the PROPKA v.2.0 program.[59]

Protonation States. Visual inspection, computed pK_a values, and experimental pH values reported for vertebrate rod photoreceptors[60] were considered in the assignment of the protonation states for all titratable residues; the cytoplasmic pH (7.29 ± 0.02) was assumed for the transmembrane and cytoplasmic domains and the intradiscal pH (6.5 ± 0.07) for residues extending into the intradiscal space. Residues Asp83, Glu122, and Glu181 were protonated in bWT, hWT, and hS186W, in accord with UV−vis spectral studies of site-directed mutants for the first two residues and FTIR experiments in bovine-WT rhodopsin.[61,62] In the hM207R mutant, Asp83 and Glu181 were protonated and Glu122 was left charged.

The protonation state of Glu181 in vertebrate rhodopsins has not been established unambiguously: NMR spectroscopic measurements,[63,64] FTIR spectra, and MD simulations[9] together with a recent QM/MM study[65] support a charged Glu181. Two-photon spectroscopy studies,[66] the 3-D crystal structure determination,[14] and site-specific mutagenesis studies involving preresonance Raman vibrational spectra of the unphotolyzed E181Q mutant[67] find Glu181 to be protonated in the dark state. QM/MM work on visual rhodopsin addressed both the neutral and charged forms of Glu181 and concluded from dipole moment analysis that Glu181 is present in its neutral form.[67] QM/MM calculations indicate that the protonation state of Glu181 does not have any crucial influence on the bond length alternation or the optical spectra.[65] Here, we use neutral Glu181.

In all cases, His100 and His211 were protonated at the δ nitrogen only. His195 was also δ protonated in bWT. His65 and His152 were always protonated at the ε nitrogen only. These histidine protonation states agree with those adopted previously.[14] His278 (intradiscal) was protonated at both nitrogen atoms. Cys316 was found to be charged in the mutants, which is not significant for the absorption in the dark state but for transducin activation.[68] Cys110 and Cys187 were unprotonated and formed a disulfide bridge in all structures. Glu113 was negatively charged and located close to the positive charge of the protonated Schiff base (RPSB) in bWT, hWT, and hM207R. This assignment for Glu113 and the Schiff-base linkage (SBL) are well established for WT rhodopsins. Experimental evidence from absorption spectra has been interpreted in terms of an unprotonated SBL in the M207R mutant,[35] but our calculations predict similar spectral behavior for a protonated SBL, and the pK_a^{SBL} value favors a RPSB. By contrast, in the hS186W mutant, the computed pK_a values (pK_a^{Glu113} = 8.31 and pK_a^{SBL} = 5.88) indicate that the salt bridge between Glu113 and SBL is broken. We have thus adopted a setup for hS186W in which Glu113 and SBL (Lys296) are both neutral. For all other amino acid residues, standard protonation states were used.

MM Optimization. All homology models were refined by energy minimizations using NAMD v. 2.7[69] with the CG algorithm. The resulting models were used as a starting point for the subsequent calculations. Two different setups were used (Figure 2), one with the protein solvated in a water sphere (model I) and the other with the protein embedded in a lipid bilayer (model II).

Structure Validation. Three different structure validation tools were used to test the reliability and internal consistency of our models. Sequence−structure compatibility was evaluated by VERIFY-3D,[70] backbone conformations were inspected by Ramachandran plots obtained from PROCHECK analysis,[71] and the 3D-model packing quality was tested by calculating the Z-score value with WHAT_CHECK.[72] The root-mean-square deviations (rmsd) between the backbones of each 3D model and the crystal structure were also checked (Table S1, Supporting Information).

Membrane Embedding. Simulations of the rhodopsin models within the membrane/water/ion environment were performed to evaluate the effect of the biological membrane on protein conformation. This approach of simulating rhodopsin within its native environment of a hydrated lipid bilayer is supported by experimental data, which show that the functionality of rhodopsins is reconstituted in artificial membranes.[73] Theoretical studies have reproduced the properties of bovine rhodopsins in membranes very well.[9] The rod outer segment disk membranes which host rhodopsin are composed of unsaturated lipids[74] and phospholipids.[6] Hence, the rhodopsins, oriented along the *z*-axis, were embedded in a rectangular patch of palmitoyl-oleoyl-phosphatidyl choline (POPC) hydrated bilayer, using VMD v. 1.8.7.[75] Additional water molecules were placed using the SOLVATE v. 1.0 program[76] for filling the empty spaces inside the pores and in their surroundings. The water molecules within the rhodopsin−membrane interface were removed. The placement of the rhodopsin within the POPC membrane was determined by the hydrophobicity of its residues; a very good membrane−protein alignment was obtained, and lipids and water molecules overlapping with the rhodopsin or palmitoyl residues were eliminated. Next, complexes were placed in a box

of water with slightly smaller size than the *xy* plane; any water molecule inside the lipid bilayer was removed. The systems were neutralized using Na^+ and Cl^- ions at physiological concentration (154 mM). The resulting rhodopsin/membrane/water/ion system with dimensions of 83 × 84 × 87 $Å^3$ contains the homology model structures, 170 POPC molecules, water molecules, and ions (Figure 2).

MD Simulations. We recall that we consider two different models: model I with the protein in a water sphere and model II with the protein in a solvated POPC lipid bilayer (Figure 2). The simulations for model I will be denoted simply by **MD**, whereas for model II we distinguish between simulations with a constrained protein in the membrane (**CMD**) and completely unconstrained simulations (**FMD**). Comparison of **CMD** and **FMD** results for model II allows us to assess the effect of large conformational changes in the RBP for a given mutant. By default, we will refer to the results obtained using model I.

MD of Solvated Rhodopsins, Model I. The MD simulations for model I were performed using the program CHARMM in version 33b1.[77,78] The MM parameters for retinal were adopted from the literature.[79] The initial set of coordinates was taken from the structures bWT, hWT, hM207R, and hS186W generated by homology modeling. SHAKE constraints[80] were applied to all bonds involving hydrogen atoms. After the initial setup, the system was solvated in a pre-equilibrated sphere of TIP3P water with radius 30 Å, located at the origin of the coordinate system (atom C11 of the 11-*cis*-retinal). A spherical quartic boundary potential acting on the O atoms of the water molecules was used. All protein atoms more than 20 Å away from the center of the coordinate system were kept frozen in all subsequent calculations. After initial placement of the water sphere, overlapping water molecules (distance between Ow and any heavy atom <2.8 Å) were deleted and all water molecules were energy-minimized in 250 cycles steepest-descent and 250 cycles ABNR (augment basis Newton−Raphson) minimizations. The positions of all non-water atoms were frozen at this stage. Thereafter, the protein atoms were restrained by a strong harmonic potential, and the protein and water molecules were minimized using the same procedure as before. After this minimization, protein and water atoms were subjected to a 15 ps constant-temperature MD with a time step of 1 fs, applying a starting temperature of 50 K, a final temperature of 300 K, and a temperature step of 10 K every 100 MD steps. Subsequently, a new water sphere was superimposed on the system, overlapping atoms were deleted, and the system was again subjected to a 15 ps MD, using weaker harmonic restraints on the protein atoms. This procedure was performed 12 times, each time lowering the harmonic restraints on the protein atoms. In the last three cycles, the equilibration time was increased to 30 ps. Finally, a 500 ps constant-temperature MD production run with a time step of 1 fs was performed. Again, the temperature was initially raised from 50 to 300 K in steps of 10 K every 100 MD steps. The VMD program was used for visualizing all the MD trajectories and resulting geometries.[75]

CMD and FMD Simulations of Rhodopsins in the Lipid Bilayer, Model II. At first, an energy minimization was performed on the complex using the CG algorithm followed by a 500 ps MD with all residues except lipid tails and palmitoyl fixed. The all-atom CHARMM force field[81,82] and the TIP3P water model[83] were employed. Periodic boundary conditions (PBC) were used. Electrostatic interactions for the full system with PBC were calculated using the Ewald particle mesh method,[84] a grid spacing of 1 Å, and a cutoff of 12 Å. The time step was 1.0 fs. An

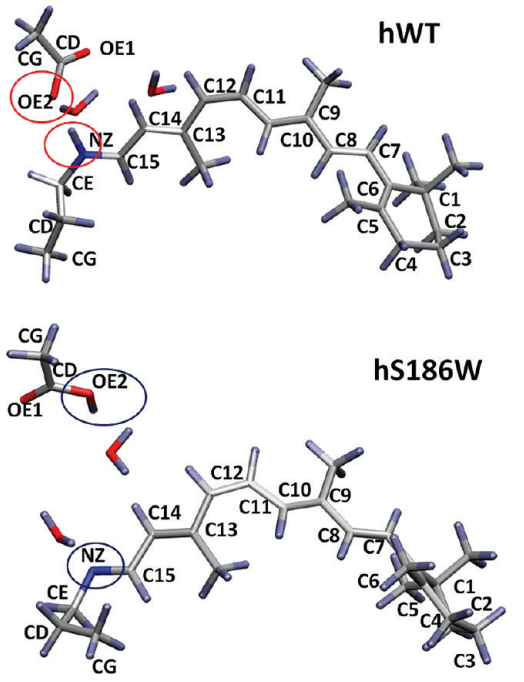

Figure 3. QM regions with labels for the non-hydrogen atoms (except for methyl groups and water molecules). Top, hWT (identical for bWT and hM207R); bottom, hS186W. The differences between the two QM regions are highlighted.

appropriate disorder of a fluid-like bilayer was induced. Thereafter, a second minimization was performed before carrying out another MD run for equilibration (500 ps at 300 K and constant pressure of 1 bar with nonfixed atoms, same conditions as in the first MD). Harmonic constraints were imposed on the protein and retinal. The hydration of the membrane−protein interface was prevented. This simulation allowed lipids, water molecules, and ions to adapt to the protein in its crystal conformation, with appropriate relaxation of the environment, in order to avoid large deviations from the X-ray structure in the backbone and chromophore regions.[85] After this constrained **CMD** procedure, an unconstrained simulation (**FMD**) was performed as follows. The system was heated up to 310 K during a constant pressure (1 bar) MD run of 500 ps with harmonic constraints released. The subsequent **FMD** simulation was run for 1.5 ns at constant pressure (1 bar) and constant area. This allowed us to identify structural deviations of the rhodopsin in the membrane environment compared with the crystal structure. All calculations for model II were performed using NAMD,[69] with a total simulation time of 3 ns.

QM/MM Structure Optimizations. QM/MM optimizations of four snapshots from the MD simulations of model I and of three snapshots from the FMD simulations of model II were performed with the program ChemShell.[86] We used Turbomole[87] in version 5.7.1 for the QM calculations and DL_POLY[88] as a driver of the CHARMM22 force field. The QM region for bWT, hWT, and hM207R (73 atoms) included the chromophore 11-*cis*-retinal, part of Lys296, part of Glu113, and two water molecules (Figure 3). The QM region for the hS186W mutant was the same (73 atoms), with one exception: one proton was shifted from NZ in Lys296 to Glu113 so that both residues were neutral (Figure 3). A second QM region was used to further evaluate the relative stability of the mutated systems: QM2 (106 atoms) includes the 73 atoms of the

standard QM region plus part of residues Glu181, Tyr268, and Thr94 (Figure S1, Supporting Information). The QM part was described using the B3LYP density functional[89−93] together with the TZVP and SVP basis sets from the Turbomole basis set library.

The QM/MM interactions were treated by an electrostatic embedding scheme.[94] Open valencies at the QM/MM border were saturated using hydrogen link atoms. To avoid overpolarization of the QM region at the boundary, we used a charge shift approach.[95,96] No electrostatic cutoffs were applied for the QM/MM interactions. Natural bond orbital (NBO) analysis was employed to characterize the electron density distribution in the QM region.

Geometry optimizations were performed using the HDLC optimizer[97] as implemented in ChemShell. They were done in hybrid delocalized internal coordinates. The coordinates of all atoms beyond 15 Å from the center (atom C11 of the 11-*cis*-retinal) were fixed. The optimization was finished when the maximum gradient component was below 0.00045 au. The VMD[75] program was used for drawing molecular structures.

Vertical Excitation Energies. We calculated vertical excitation energies, oscillator strengths, and dipole moments in the protein environment at the QM/MM level using the combined density functional multireference configuration interaction (DFT/MRCI) method of Grimme and Waletzke.[49] Time-dependent DFT (TDDFT)[50−53,98] calculations were also carried out for the sake of comparison. The same QM/MM conventions were used as in the optimizations (see above). The DFT/MRCI method takes major parts of the dynamic electron correlation into account by DFT, while static correlation effects are included by a short CI expansion. The configuration state functions in the MRCI expansion are built up from Kohn−Sham orbitals of a closed-shell reference state. The effective DFT/MRCI Hamiltonian contains five empirical parameters, which depend only on the multiplicity of the excited state, the number of open shells of a configuration, and the density functional employed. Optimized parameter sets[49] are available for the DFT/MRCI Hamiltonian in combination with the BH-LYP functional.[89,90,92,93,99] We used a modified set of parameters recently developed in the Grimme group[100] (p_1 = 0.629, p_2 = 0.611, p_J = 0.119, $p[0]$ = 8.000, α = 0.503). The required DFT wave functions were generated by Turbomole, version 5.71. Using standard parameters, the

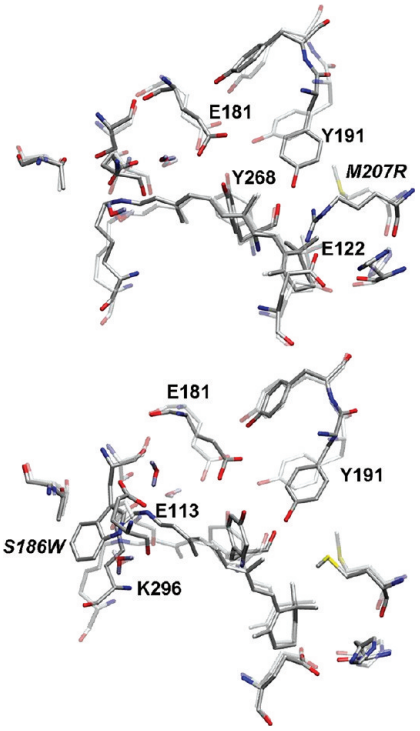

Figure 5. Changes in the rhodopsin binding pocket of hM207R (top) and hS186W (bottom) compared with hWT (transparent). Hydrogen atoms (except for water) are omitted, and important residues are highlighted. The structures are QM/MM optimized snapshots.

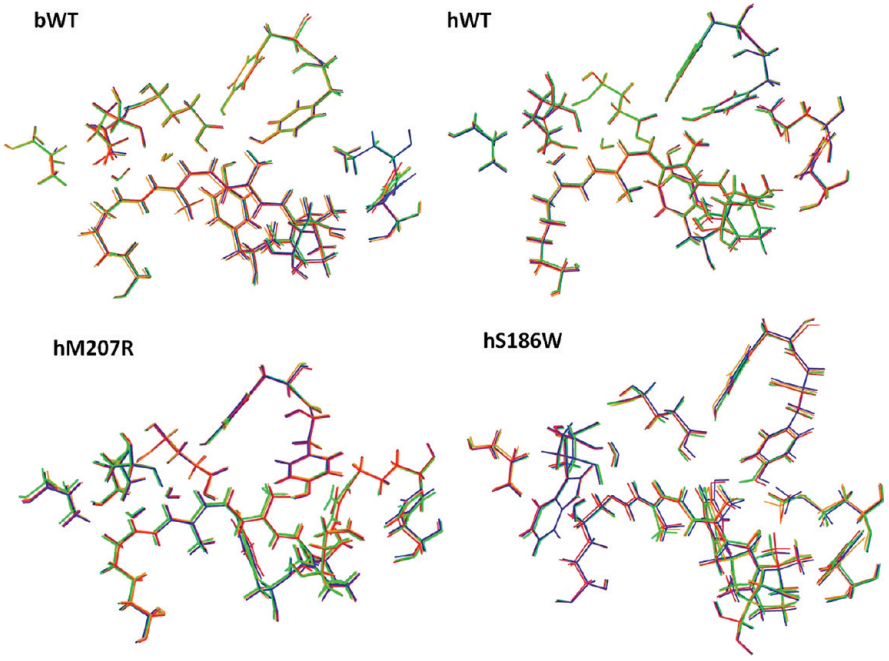

Figure 4. Overlay of the rhodopsin binding pocket in the QM/MM optimized snapshots of the solvated protein systems, for the wild-type structures (top) and the mutants (bottom).

dx.doi.org/10.1021/jp2037334 |*J. Phys. Chem. B* 2012, 116, 1060–1076

DFT/MRCI method yields vertical excitation energies which are typically within 0.2 eV of the experimental values.[49,101]

RESULTS AND DISCUSSION

Structural Aspects. For each of the four rhodopsins (bWT, hWT, hM207R, and hS186W), QM/MM geometry optimizations have been carried out for four snapshots (model I). For a given rhodopsin, the geometries in the RBP are basically the same in all four snapshots (Figure 4). As expected, the hydrogen bond network around the chromophore is distorted in the two mutants compared with the WT rhodopsins (Figures 5 and 6). This is related to the substitution of the neutral methionine residue by the charged arginine residue in hM207R and of serine by tryptophan in hS186W. In the solvated rhodopsin (model I), the mutation M207R brings residues Glu113, Ser186, and Thr94 closer to each other (compared with hWT), disrupts the hydrogen bond interactions of Glu181 with Tyr191 and Tyr192, and leads to an elongation of the $O_{Tyr268}-O_{Tyr191}$ and $O_{Ser186}-O_{W6}$ distances. The mutation S186W results in the loss of the interactions between Glu113 and Lys296; in addition, Glu113 and Thr94 move away from each other (compared with hWT), and the hydrogen bond network between Glu181, W6, and Tyr191 is also affected in hS186W (Table 1).

The energetic consequences of these mutations can be estimated by single-point QM (B3LYP/TZVP) calculations on the QM region at the QM/MM optimized geometries. The corresponding average values for the absolute and relative energies are given in Table 2. Compared with hWT, the QM region (73 atoms) is notably less stable in hM207R (by 6.5 kcal/mol), whereas the effect is much smaller in hS186W (0.8 kcal/mol) in spite of the loss of the salt bridge between Lys296 and Glu113. In addition, QM/MM geometry optimizations (B3LYP/SVP) with a larger QM region (QM2) and a smaller basis (SVP from the Turbomole basis set library) were performed for two snapshots of each system. As mentioned above, QM2 (106 atoms) included the 73 atoms of the standard QM region plus residues Glu181, Tyr268, and Thr94 (see Figure S1, Supporting Information). We found that QM2 of hM207R is much less stable than QM2 of

Table 1. Average Heavy-Atom Hydrogen Bond Distances (Å) from QM/MM Optimizations (Model I) between Residues in the Rhodopsin Binding Pocket

	QM/MM (model I)		
	hWT	hM207R	hS186W
$OE2_{Glu113}-NZ_{Lys296}$	2.71 ± 0.01	2.73 ± 0.02	6.61 ± 0.07
$OE1_{Glu113}-NZ_{Lys296}$	3.76 ± 0.05	3.50 ± 0.03	6.64 ± 0.10
$OE2_{Glu113}-O_{W8}$	2.76 ± 0.00	2.81 ± 0.02	3.86 ± 0.12
$OE2_{Glu113}-OG_{Ser186}$	5.42 ± 0.03	4.28 ± 0.05	
$OE2_{Glu113}-OG1_{Thr94}$	4.50 ± 0.05	3.96 ± 0.06	6.29 ± 0.09
$OE2_{Glu181}-O_{w6}$	2.74 ± 0.01	2.77 ± 0.01	4.26 ± 0.08
$OE2_{Glu181}-OH_{Tyr268}$	2.78 ± 0.02	2.80 ± 0.02	2.90 ± 0.05
$OE1_{Glu181}-OH_{Tyr192}$	2.89 ± 0.01	4.86 ± 0.06	2.68 ± 0.02
$OE1_{Glu181}-OH_{Tyr191}$	2.78 ± 0.02	5.80 ± 0.13	5.00 ± 0.25
$OH_{Tyr268}-OH_{Tyr191}$	2.90 ± 0.05	4.70 ± 0.12	2.91 ± 0.06
$OG_{Ser186}-OG1_{Thr94}$	4.95 ± 0.03	2.85 ± 0.01	
$OG_{Ser186}-O_{W6}$	2.76 ± 0.00	4.21 ± 0.04	

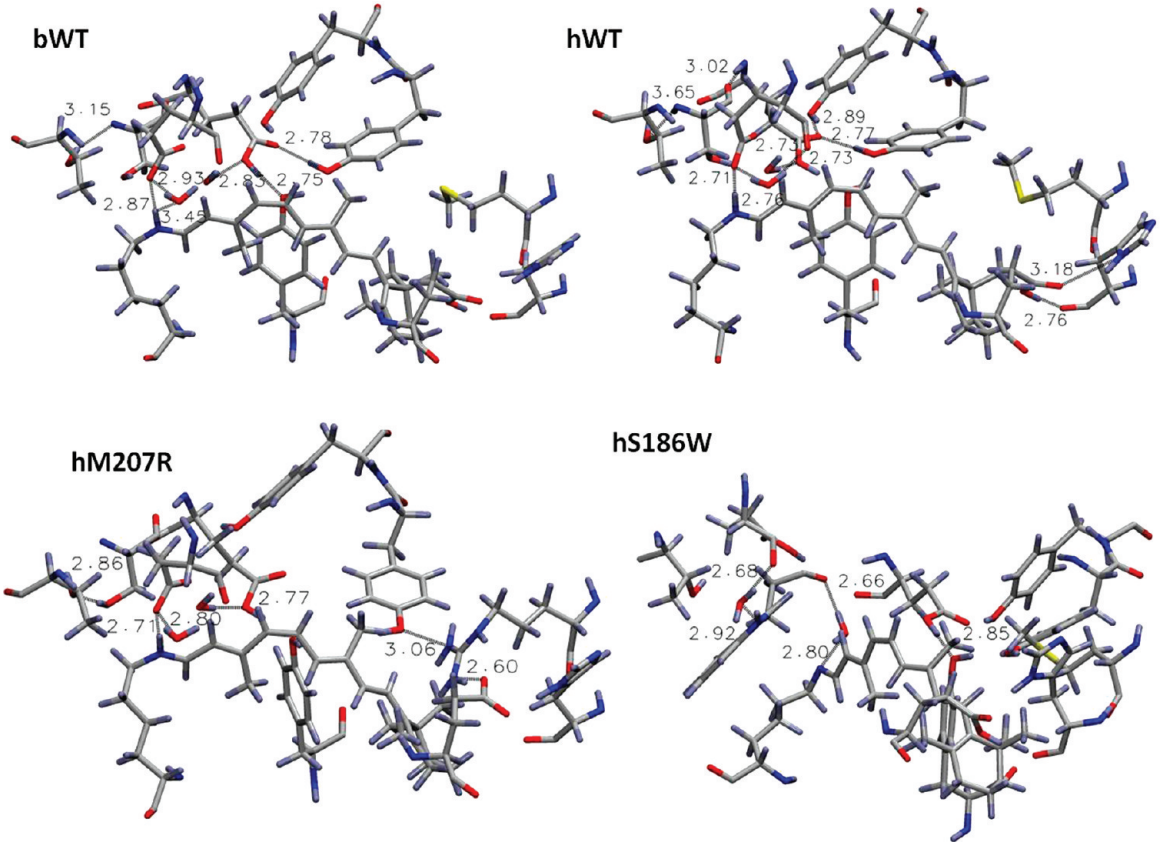

Figure 6. Hydrogen bonding in the rhodopsin binding pocket. Key heavy-atom distances are given in Å.

dx.doi.org/10.1021/jp2037334 |J. Phys. Chem. B 2012, 116, 1060–1076

hWT (by 29.5 kcal/mol), while QM2 of hS186W is only slightly less stable (by 3.7 kcal/mol). Finally, a tentative evaluation of the MM (NAMD) energies of the QM region plus the neighboring Glu181, Tyr191, Tyr192, Tyr268, and Thr94 residues also indicates a possible destabilization of the retinal binding pocket in the mutants with respect to hWT (see Figure S1a, Supporting Information). This is consistent with recent protein folding studies that indicate some destabilization of the whole protein due to mutation.[23]

Table 2. Average Absolute and Relative Energies (kcal/mol) of the QM Regions in the Human Wild Type Rhodopsin hWT and the Mutants hM207R and hS186W (See Text)

	B3LYP/TZVP		B3LYP/SVP
	QM		QM2
structure	energy	relative energies	relative energies
hWT	−837036.65	0	0
hM207R	−837030.12	6.5	29.5
hS186W	−837035.85	0.8	3.7

In the following, we compare the optimized structures for the four rhodopsins in more detail. We focus on four aspects: the similarity between the rhodopsin binding pockets, the $C_{11}-C_{12}$ double bond in the dark state, the planarity of the β-ionone ring of retinal, and the bond length alternation (BLA) in the unsaturated polyene chain. The validity of the 3D models and energetic aspects are addressed in the Supporting Information. Generally speaking, our analysis shows a pronounced similarity between the two wild-type structures and reveals some characteristic changes in the two mutant structures.

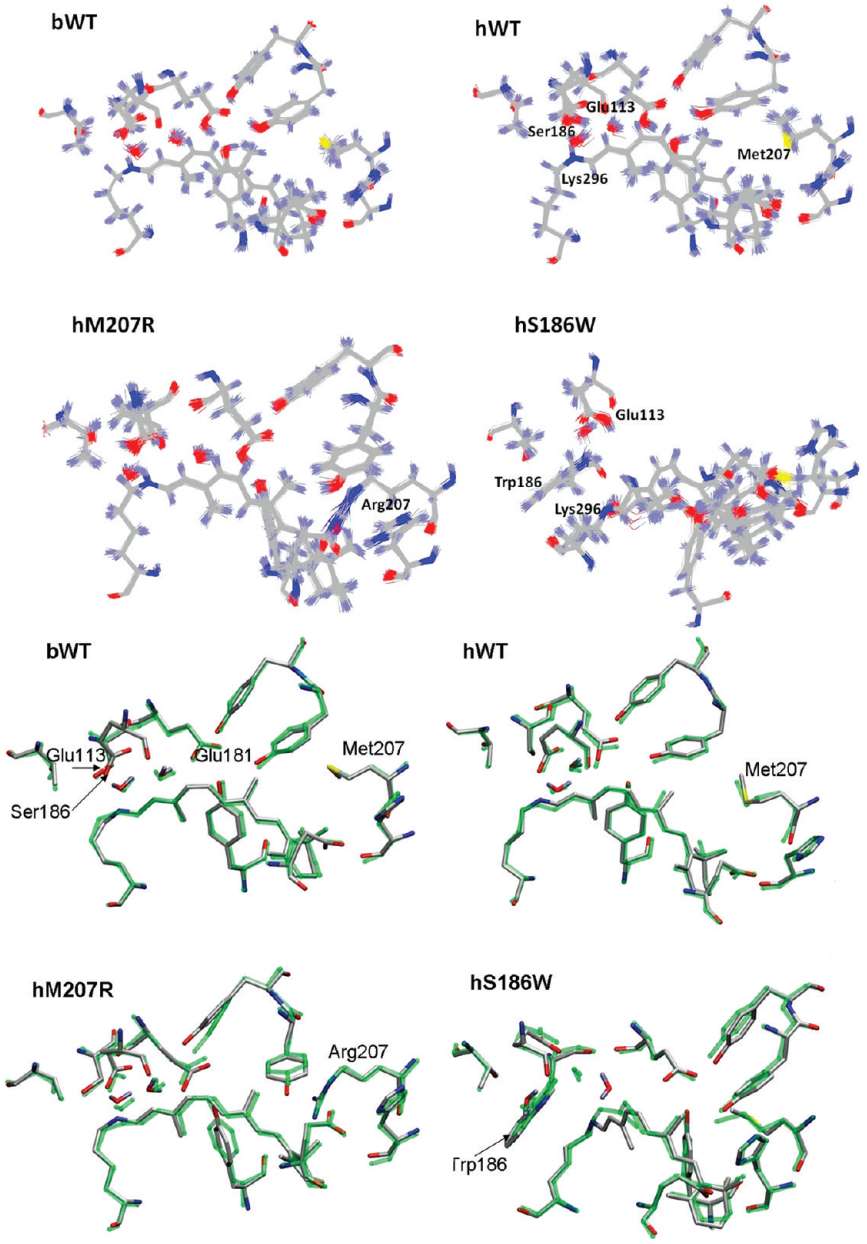

Figure 7. Top: Overlay of rhodopsin binding pockets from MD simulations of model I (solvated protein). Bottom: Overlay between snapshots from MD simulations of model I and CMD simulations of model II (constrained protein in the membrane).

dx.doi.org/10.1021/jp2037334 |J. Phys. Chem. B 2012, 116, 1060–1076

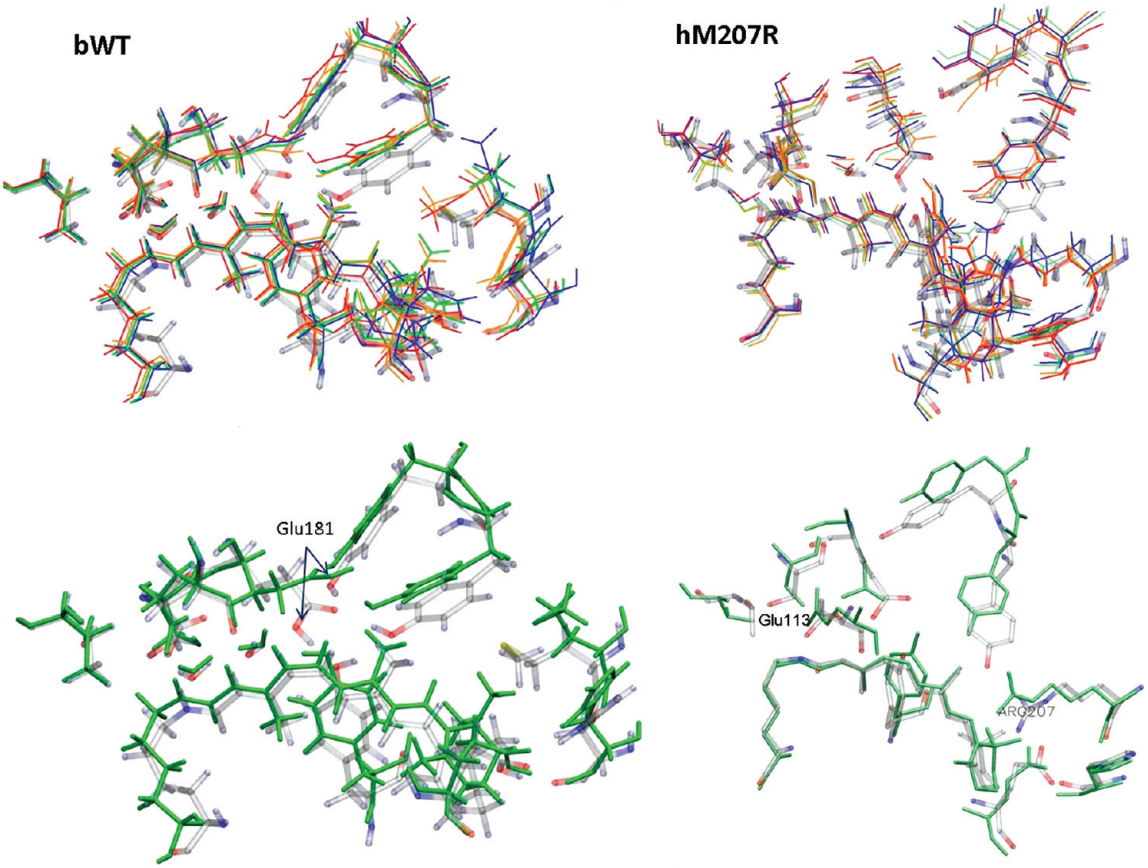

Figure 8. Overlay of the rhodopsin binding pockets of bWT and hM207R from snapshots of the unconstrained membrane FMD simulation (model II) and from one QM/MM optimized snapshot of the solvated protein MD simulation (model I). Color code: model II: red, 250 ps; green, 370 ps; orange, 500 ps; blue, 1 ns; model I: transparent licorice. Top panel: overlay of all structures. Bottom panel: FMD snapshot after 370 ps vs QM/MM optimized geometry; for a better view, hydrogen atoms are omitted in hM207R (bottom right).

Similarity between Rhodopsin Binding Pockets (RBPs). Conformations obtained from the classical CMD trajectories of model II (protein in the membrane) have RBPs very similar to those from the MD trajectories of model I (solvated protein); see Figure 7 and Figure S4, Supporting Information. The geometries of the residues in the RBP, the conformation of the 11-*cis*-retinal, and the hydrogen bonds relevant to the spectroscopic properties are well conserved in the retinal binding sites of the CMD and MD structures.

On the other hand, significant conformational changes from the starting geometry (and from the crystal structure) are found after the first nanosecond of the unconstrained FMD simulation of model II. This is not surprising, since extensive deviations from the crystal structure have been reported in other membrane–rhodopsin simulations.[102]

Perhaps one of the most interesting changes during the FMD runs is that Glu181 in bWT moves its carboxylic group away from retinal (Figure 8, bottom left, and Figure S2, Supporting Information) to adopt a position not encountered during the MD and CMD simulations (Figures 7 and 8). Another important change is that the Arg207 guanidino group in hM207R adopts a position away from the cyclohexenyl ring of retinal (Figure 8, bottom right) in contrast to the MD and CMD structures in which this group points to the ring (Figures 7 and 8 and Figure S2, Supporting Information). Therefore, the hydrogen-bonding network at the retinal binding site is distorted in both the hM207R and hS186W mutants (Table 1, Figures 5 and 6, and Figure S4, Supporting Information).

$C_{11}-C_{12}$ Double Bond in the Dark State. The dihedral angle $\varphi C_{10}-C_{11}-C_{12}-C_{13}$ characterizes the structure around the $C_{11}-C_{12}$ double bond. The corresponding conformation is 11-*cis* for all structures. The wild type rhodopsins (bWT and hWT) have a dihedral angle of $-12°$, in agreement with the values of -11, -17, and $-16°$ reported in theoretical studies for the dark state of bovine structures.[103,104] A recent QM/MM study on squid rhodopsin also finds that a negative pretwist ($-17°$) is required for the photoisomerization of the $C_{11}-C_{12}$ double bond.[105] In contrast to the WTs, the values for the hM207R and hS186W mutants are around $-9°$ (Table 3). Apparently, the protein environment in the WT rhodopsins exerts a stronger steric strain on the 11-*cis*-retinal moiety and thus enforces a somewhat larger twist around the $C_{11}-C_{12}$ double bond which will support the $C_{11}-C_{12}$ photoisomerization. By the same token, one may expect that this photoisomerization will be less facile in the mutants. Such environmental effects are important because the electronic structure of retinal is unselective toward the rotation of the double bonds in the polyene chain,[106] so that the protein environment is decisive for a selective isomerization. However, the energetic consequences of small variations in the dihedral angle $\varphi C_{10}-C_{11}-C_{12}-C_{13}$ are small: changing this angle by about 5° (to $-7.5°$ in hWT and nearly $-14.5°$ in hM207R and hS186W) and performing constrained QM/MM

Table 3. Dihedral Angle $\varphi C_{10}-C_{11}-C_{12}-C_{13}$ in the Dark State of Retinal (deg), Bond Length Alternation (BLA, Å), Dipole Moment (D) of the S_0 and S_1 States (μ_{S_0} and μ_{S_1}) of the QM Region, and Difference $\mu_{S_1} - \mu_{S_0}$ (D) in the Wild-Type Rhodopsins and Mutants

structure	$\varphi C_{10}-C_{11}-C_{12}-C_{13}$[a]	BLA	μ_{S_0}	μ_{S_1}	$\mu_{S_1} - \mu_{S_0}$
bWT	−12.04 ± 0.74	0.42 ± 0.00	14.44 ± 0.56	25.57 ± 0.91	11.13 ± 0.38
hWT	−12.21 ± 0.45	0.43 ± 0.01	15.65 ± 0.63	27.17 ± 0.67	11.52 ± 0.16
hM207R	−9.18 ± 0.67	0.50 ± 0.01	11.57 ± 0.21	20.51 ± 0.50	8.49 ± 0.31
hS186W	−8.57 ± 1.16	0.56 ± 0.02	11.90 ± 0.27	24.38 ± 1.11	12.48 ± 1.01

[a] In the crystal structure (pdb 1U19), the value of $\varphi C_{10}-C_{11}-C_{12}-C_{13}$ is −36.12°.[14]

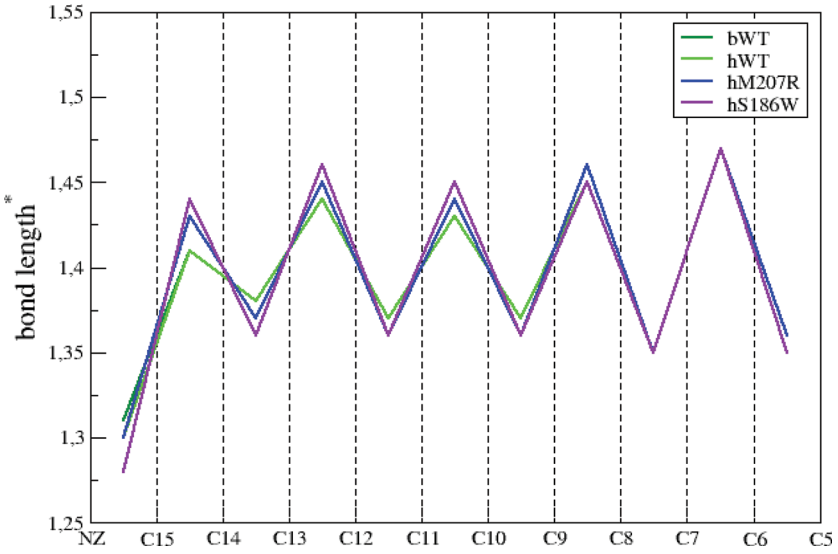

Figure 9. Bond length alternation in the ground state of the wild-type and mutant rhodopsins. The bond lengths are given in Å (see Figure 3 for numbering).

optimizations with this angle fixed leads to changes of less than 0.6 kcal/mol in the relative energies. Hence, the smaller twist in the mutants imposes only a minor energetic penalty to the $C_{11}-C_{12}$ photoisomerization.

Twist and Planarity of the β-Ionone Ring of Retinal. The orientation of the β-ionone ring is *6-s-cis* at the C_6-C_7 bond. The calculated values of the dihedral angle $\varphi C_5-C_6-C_7-C_8$ are bWT (−48.1 ± 1.5°), hWT (−43.4 ± 1.4°), hM207R (−36.9 ± 1.5°), and hS186W (−44.6 ± 3.9°). Here and in the following, we give the mean value and the standard deviations over the four chosen snapshots. The computed dihedral angles are in good agreement with the experimental value for chain B in the 1U19 crystal (−31.9°)[14] and with results from previous ONIOM-EE (B3LYP/6-31G*:AMBER) calculations (−44°),[103] classical MD simulations (−52°), and QM/MM MD studies (−42°).[104] The *6-s-cis* conformation has been found by all X-ray studies of bovine rhodopsin[14] to be the preferred conformation in this protein.[12] Recent QM/MM calculations on squid rhodopsin also give an intermediate value of −45° for the $\varphi C_5-C_6-C_7-C_8$ dihedral angle.[107] This study reports the *6-s-cis* conformation of 11-*cis*-retinal as the most stable one for squid and bovine rhodopsins,[107] in agreement with the orientation of the β-ionone ring in our calculations.

Another important geometrical parameter of retinal is the dihedral angle ($\varphi_\omega C_4-C_5-C_6-C_7$) of the β-ionone ring which is related to its planarity. The calculated values of 178.7 ± 0.7° (bWT), 177.4 ± 0.4° (hWT), −178.9 ± 0.3° (hM207R), and 177.0 ± 0.7° (hS186W) agree well with the crystal structure[14] (170.6°), although they are slightly higher and thus closer to planarity.

Bond Length Alternation. The bond length alternation (BLA) in the polyene chain has been related to the spectral tuning by the protein environment.[12,104,108] It is calculated as the sum of all formal single-bond lengths minus the sum of all formal double-bond lengths along the conjugated carbon chain between the C6 and N atoms.[104] The BLA values for the bovine rhodopsin structure are well documented[12,14,104] and in full agreement with our results for the bWT system (Table 3 and Figure 9).

The average BLA values for the mutants hM207R (0.50 Å) and hS186W (0.56 Å) are higher than those for the wild type systems (0.42−0.43 Å); see Table 3. Differences between BLA values have previously been related to differences in the electronic structure.[12,14,104] In retinals with higher BLA values, the highest occupied molecular orbital (HOMO) tends to be more localized in the ionone ring region.[12] The BLA is also influenced by the electrostatic effect of the counterion Glu113, and it correlates with the ground-state dipole moment (μ),[104] the vertical excitation energies,[12] and the positive charge along the polyene chain (the higher the positive charge, the higher the BLA).[13] The larger BLA values in the mutants hM207R and hS186W (by 0.08 and 0.14 Å, respectively) thus indicate less delocalization of the electron density in the conjugated chain (Table 3, Figure 9) and are consistent with the blue shifts of the vertical excitation energies found in both cases. Recent QM/MM studies[105,107]

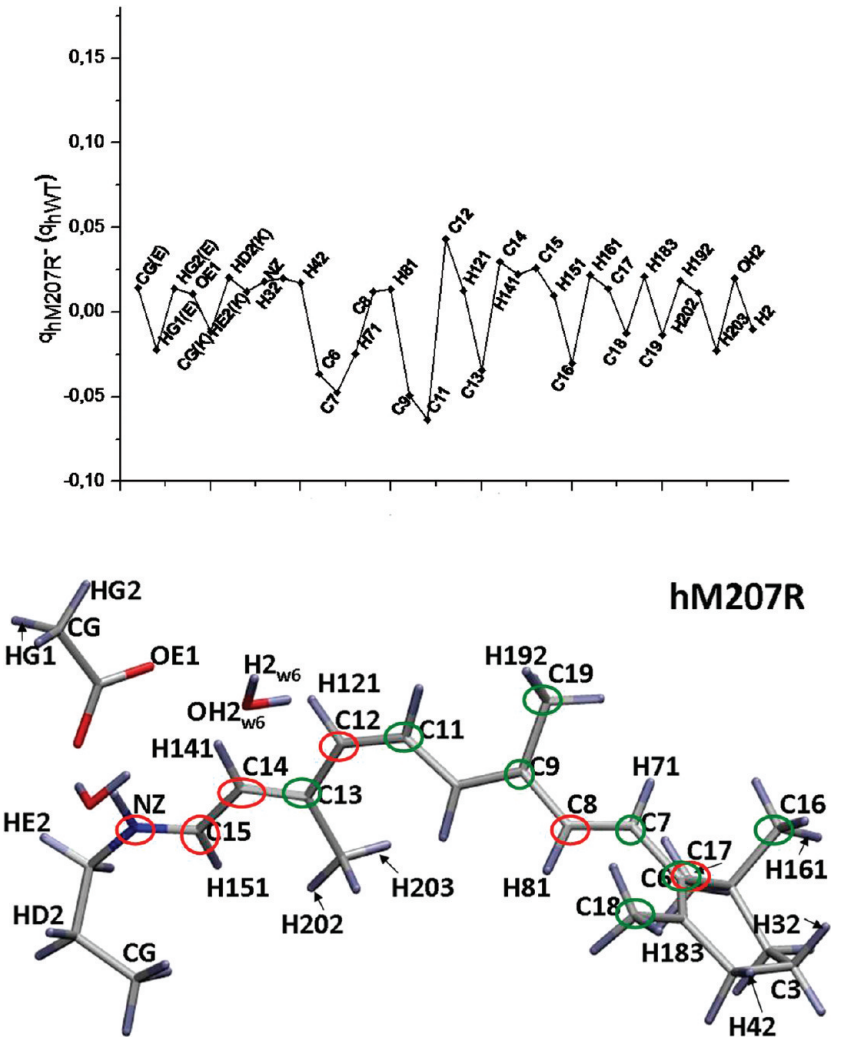

Figure 10. Top: NBO charge differences between hM207R and hWT (exceeding 0.01 *e* in absolute value). Bottom: Atom labels; red (green) marks indicate decreasing (increasing) electron density.

show significant deviations between the BLA values of squid and bovine rhodopsin, which correlate with the larger blue shift found in these systems. In our case, the changes in the BLA values are smaller and, consequently, the blue shift of the vertical excitation energies is less pronounced. There are some interesting similarities between the BLA patterns in our work and in squid rhodopsin. The highest peak in our BLA plot for hWT (Figure 9) corresponds to the C_6-C_7 bond (~1.47 Å), and the lowest one to the $C_{14}-C_{15}$ bond (~1.41 Å), in complete analogy to the BLA analysis for squid rhodopsin with values of 1.47 Å for C_6-C_7 and 1.40 Å for $C_{14}-C_{15}$ bonds.[105] These similarities (with regard to $\varphi C_5-C_6-C_7-C_8$, $C_{11}-C_{12}$, and BLA) between systems otherwise so different should be taken into account in further studies of the spectral tuning mechanisms of invertebrate and vertebrate rhodopsins.

Dipole Moments and Charge Distributions. In the mutants, the dipole moment (μ) of the QM region in the ground state S_0 (μ_{S_0}) is significantly smaller than that in the wild-type proteins (Table 3). In hM207R, the chromophore is more polarized than in hWT because the replacement of Met207 by Arg207 introduces a positive charge near the ionone ring and thus induces a shift of electron density along the chromophore chain in this direction (Figure 10). The deprotonated Glu122 residue adopts an orientation in hM207R somewhat different from that in hWT (Figure 5), but its carboxylate group is involved in hydrogen bonds with the surrounding residues and thus has less of an effect on the chromophore charge distribution. The electron densities on the C12, C14, C15, and NZ atoms of the chromophore and of the oxygen atom of W6 are lower in the mutant than in hWT (see Figure 10 and the NBO charges in Table S3, Supporting Information). A similar trend is also found for the hS186W system, in which the electron densities on the C12, C14, and C20 atoms are lower than those in hWT. Since there is no charged residue interacting with the ionone ring like in the case of hM207R, the electron density on the C16 and C18 carbon atoms in hS186W (see Figures 10 and 11) is not affected. Given that the Schiff base is unprotonated in hS186W, the electron density on atoms NZ and C15 is also not affected. However, a remarkable decrease of the electron density is found for the OE2 and OE1 oxygen atoms of Glu113 in hS186W in agreement with the change of the protonation state of this residue from charged to neutral.

It is obvious from the form of the frontier orbitals (Figure 12) that the HOMO−LUMO excitation in these rhodopsins leads

dx.doi.org/10.1021/jp2037334 |*J. Phys. Chem. B* 2012, 116, 1060–1076

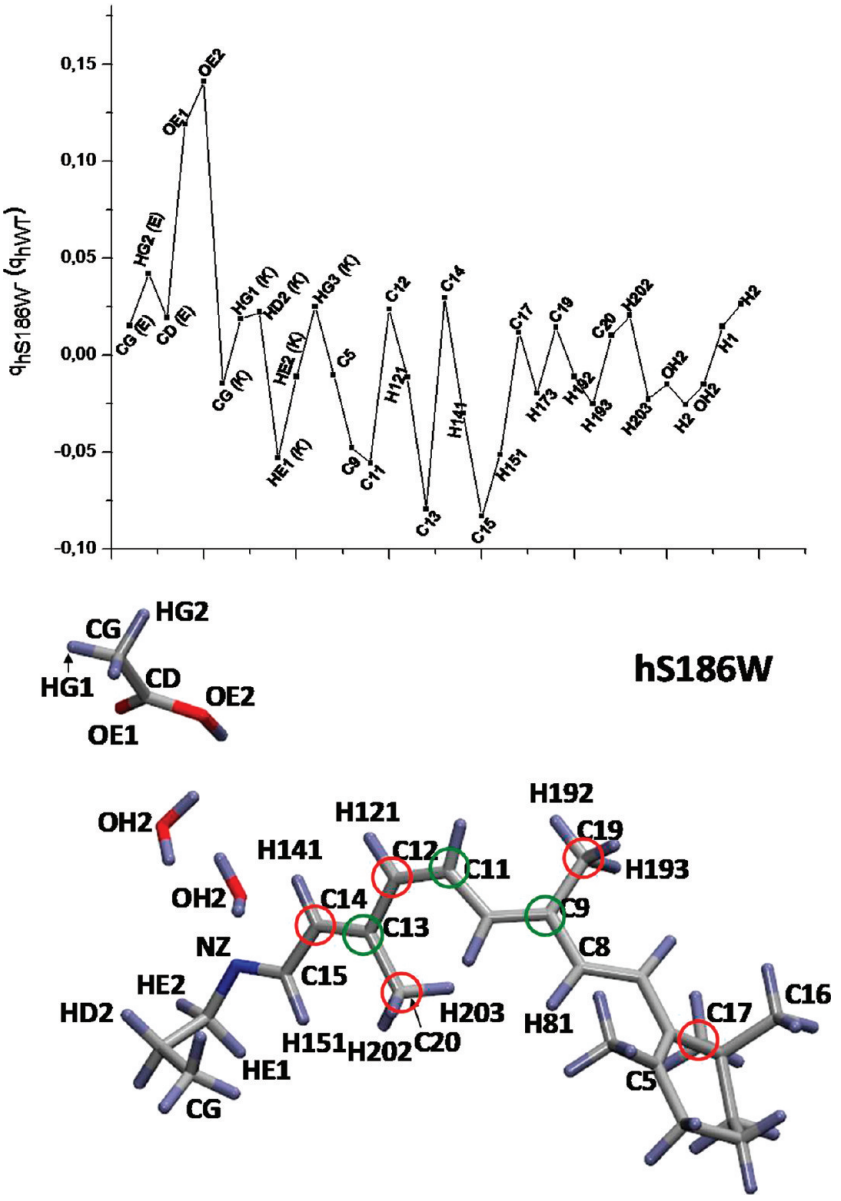

Figure 11. Top: NBO charge differences between hS186W and hWT (exceeding 0.01 *e* in absolute value). Bottom: Atom labels; red (green) marks indicate decreasing (increasing) electron density.

to an overall charge transfer from the ionone side (C5−C10) to the SBL side (C12−C15) of the polyene (Figure 3), i.e., toward the negatively charged Glu113 counterion, which causes an increase of dipole moment in the first excited state (S_1) compared with the S_0 ground state[109] (Table 3). In hM207R, the positive charge of the Arg207 guanidino group hinders this charge transfer upon excitation, which results in a smaller excited-state dipole moment and also in a smaller change of dipole moment ($\mu_{S_1} - \mu_{S_0}$) relative to the wild-type proteins (Table 3). In addition, although the $OE2_{Glu113}$−NZ_{Lys296} salt bridge has a similar average distance in hM207R and in the wild-type structures (2.61 ± 0.08 Å, MD simulations, model I), the OE1 oxygen atom of Glu113 is closer to retinal (NZ atom) in hM207R (3.84 ± 0.14 Å vs 2.96 ± 0.12 Å for hWT and hM207R, respectively; see Table S6, Supporting Information), which will also tend to diminish the excited-state charge transfer. Our results are in agreement with studies of the bovine-rhodopsin E122Q mutant that report a decrease of the electron transfer from the methyl group attached to the C1 atom to the nitrogen atom of the RPSB as a consequence of the negative charge around being split due to the mutation.[12]

The hS186W mutant also has a ground-state dipole moment (μ_{S_0}) that is smaller than those of the wild-type rhodopsins (Table 3). This mutant is less polar in general, since it contains a neutral SBL moiety and a neutral Glu113 residue at a relatively large distance (Table 3 and Figure 3). In the absence of a negative charge on Glu113 (as in the other three systems) and of a positive charge on residue 207 (as in hM207R), there is no special impediment against the charge shift upon HOMO−LUMO excitation (see above), and hence the change of dipole moment ($\mu_{S_1} - \mu_{S_0}$) is largest in hS186W.

Vertical Excitation Energies. Table 4 lists the vertical excitation energies and oscillator strengths of the first excited state (S_1) for all four proteins (results for the S_2 state are shown in Table S4,

dx.doi.org/10.1021/jp2037334 |*J. Phys. Chem. B* 2012, 116, 1060–1076

Supporting Information). The calculated average S_1 vertical excitation energies of the wild-type rhodopsins (2.49 eV for bWT and hWT with TDDFT, 2.56 eV for bWT, and 2.50 eV for hWT with DFT/MRCI) are in very good agreement with the experimental data (2.49 eV)[66] and with previous calculations of the optical spectra of bovine rhodopsin.[12,103,108,110] In the two mutants, the excitation energies from DFT/MRCI are ca. 0.3 eV higher than those from TDDFT—the latter are generally regarded as less reliable, and therefore, we primarily discuss the DFT/MRCI results in the following. The first vertical excitation energies are blue-shifted in both mutants with respect to hWT (2.93 eV for hM207R and 3.05 eV for hS186W vs 2.50 eV in hWT); see Table 4 and Figure S8, Supporting Information. Experimentally, the reported hypsochromic shift[35] of the first band in hM207R (3.27 eV) is even stronger than computed. It has been suggested that this indicates the presence of an unprotonated SBL in this mutant,[35] since the bovine wild-type rhodopsin also has a band at 3.27 eV when the SBL is unprotonated.[6] On the other hand, a blue shift of the first absorption band can also be caused by amino acid substitutions in the rhodopsin binding pocket, rather than by a change of the protonation state of SBL. For example, according to our DFT/MRCI calculations, both the hS186W mutant with unprotonated SBL and the hM207R mutant with protonated SBL show comparable blue shifts (3.05 and 2.93 eV vs 2.50 eV in hWT). We thus see no reason to revise our assignment of protonation states on this basis—the calculated pK_a^{SBL} values clearly support a protonated SBL moiety in hM207R (Table S5, Supporting Information) that gives rise to a Glu113−RPSB salt bridge (Table 3).

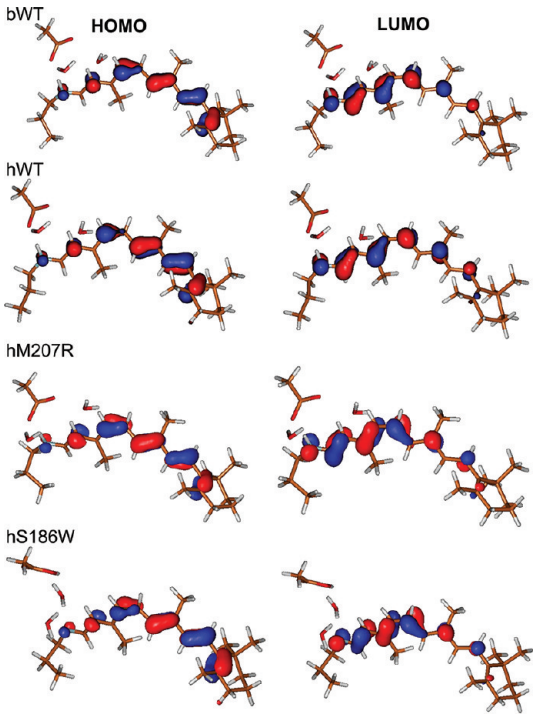

Figure 12. HOMO and LUMO orbitals (B3LYP/TZVP) for optimized snapshots.

It has been shown previously that the negatively charged groups in the binding pocket of the wild-type rhodopsins cause a significant blue shift in the S_1 excitation energy because the charge transfer upon HOMO−LUMO excitation has to overcome the electric field of the counterion.[108] This effect is intensified in the hM207R mutant due to the stronger electric field of the counterion compared with hWT: the blue shift of 0.43 eV can be seen as a consequence of the electronic polarization of the Arg207 guanidino group and the strong electrostatic influence of the anionic Glu113 residue. The latter is larger in hM207R that in the wild-type structures (since Glu113 is closer to the RPSB, Table 3), and hence, the S_1 state is more destabilized which results in a larger excitation energy. A similar analysis of the effect of Glu113 has been used before to explain blue shifts in bovine rhodopsin.[110] The increased electrostatic influence of Glu113 in hM207R is also reflected in the calculated dipole moments and BLA values (see Table 3 and the discussion above). The positive correlation between BLA values and vertical excitation energies and the role of electrostatic effects are well-known.[111]

In hWT, the S_0-S_1 ($\pi\pi^*$) transition is dominated by the HOMO−LUMO excitation (about 85%). In the mutants, this excitation contributes somewhat less (79% in hM207R and 84% in hS186W), and double excitations become more relevant; in

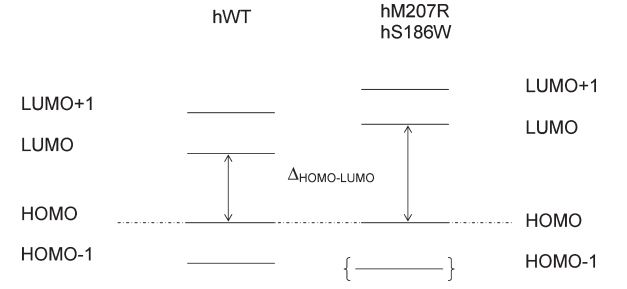

Figure 13. Schematic representation of the variation of orbital energy gaps upon mutation. The HOMO energy is taken as a reference in all cases. Compared with hWT, the HOMO−1 energy is lower in hS186W and slightly higher in hM207R.

Table 4. Average DFT/MRCI and TDDFT Vertical Excitation Energies E (eV) for the S_1 State, Associated Wavelengths (nm, in Parentheses), and Oscillator Strengths f for Snapshots from the MD Simulation of the Solvated Protein[a]

		DFT/MRCI		TDDFT	
structure	exp. value	E	f	E	f
bWT	2.49 (498)[66]	2.56 ± 0.03 (484 ± 7)	1.28 ± 0.02	2.49 ± 0.03 (497 ± 5)	0.63 ± 0.41
hWT		2.50 ± 0.05 (496 ± 10)	1.26 ± 0.02	2.49 ± 0.03 (498 ± 6)	1.05 ± 0.02
hM207R		2.93 ± 0.01 (424 ± 2)	1.22 ± 0.02	2.64 ± 0.06 (469 ± 11)	0.00 ± 0.00
hS186W		3.05 ± 0.03 (407 ± 3)	1.07 ± 0.07	2.79 ± 0.04 (445 ± 6)	0.82 ± 0.10

[a] Note that TDDFT erroneously predicts a dark S_1 state in hM207R. In the case of bWT, the TDDFT calculations yield a different state ordering in different snapshots.

Table 5. Optimized Dihedral Angles (deg) φ_1 ($H_7-C_7-NZ_{Lys296}-HZ_{Lys296}$) and φ_2 ($H_7-C_7-NZ_{Lys296}-CE_{Lys296}$) in the Human Wild-Type Rhodopsin and the Mutants (see Figure *10* for Atom Labels) for the Standard QM/MM Setup (Model I, ref) and for the Model Systems 1−4 (See Text)[a]

	hWT		hM207R		hS186W
	φ_1	φ_2	φ_1	φ_2	φ_2
ref	−49	147	−80	110	136
1	−55	141	−76	109	136
2	−20	164	not computed		164
3	−46	144	−62	115	123
4	−79	131	−74	109	124

[a] Starting geometries for the geometry optimizations: For each of the three proteins, the initial geometry obtained during system setup was used for the entries ref, 1, 3, and 4, whereas the starting geometries for 2 were generated by removing in the optimized standard QM/MM geometries (ref) all those atoms that are not present in the gas-phase model system 2.

addition, there is some more involvement of the HOMO−1 (π) and LUMO+1 (π^*) orbitals. Both mutations increase the HOMO−LUMO and HOMO−LUMO+1 gaps (Figure 13), which leads to blue shifts in the vertical excitation energies (with respect to hWT). Additionally, in both mutants, the electron density of the HOMO in the $C_{11}-C_{12}$ and $C_{10}-C_9$ bonds is higher than in hWT. In hS186W, the contribution of the β-ionone ring to the HOMO is larger than in hWT (Figure 12), as also indicated by the BLA calculated for this system.

In the hS186W mutant, Glu113 is uncharged and the salt bridge between Glu113 and the retinal is broken so that the electron density is less localized than in hM207R. This is consistent with studies on bovine wild-type rhodopsin without counterion,[110,112] which reported a massive flow of negative charge from the conjugated carbon chain toward the positive nitrogen atom following excitation. The higher vertical excitation energies calculated for both mutants are consistent with the stronger BLA found for the mutants with respect to the WT structures (Figure S3, Supporting Information).

Spectral Tuning Mechanisms in the Mutants. To evaluate the effect of the distortion of the retinal geometry, the protein environment, and the counterion on the spectral tuning in hWT and its mutants, we performed additional model calculations using B3LYP/TZVP as QM treatment.

(1) QM/MM calculations on the full system with a smaller QM region (QM0) containing only retinal and part of Lys296 (protonated in hWT and hM207R; unprotonated in hS186W).
(2) Gas-phase QM calculations on QM0 without any MM environment.
(3) QM/MM calculations analogous to (1) but with all MM point charges set to zero except those of Glu113 (retained).
(4) QM/MM calculations analogous to (1) with all MM point charges retained except those of Glu113 (set to zero).

The dihedral angle φ_1 ($H_7-C_7-NZ_{Lys296}-HZ_{Lys296}$) (Figure 3) has been used before to represent the overall twist of the retinal backbone.[74] For our standard QM/MM setup (model I), this angle is computed to be −43° for bovine rhodopsin (bWT), in good agreement with a previously reported value (−50°).[74] It is similar in hWT (−49°) but much more negative in hM207R (−80°), indicating that 11-*cis*-retinal is more twisted in this mutant (Table 5). Since φ_1 is not defined in hS186W (Lys296 is deprotonated), we also use φ_2 ($H_7-C_7-NZ_{Lys296}-CE_{Lys296}$) to measure the twist of the retinal backbone. According to the φ_2 values for the standard QM/MM setup, the hS186W mutant is twisted slightly more than hWT but significantly less so than hM207R (Table 5). Turning to the model systems (1−4), we find that the replacement of our standard QM region (retinal, Lys296, Glu113, and two water molecules) by the smaller QM0 region (see above) does not affect the overall twist of retinal much (see entry 1 in Table 5). By contrast, the gas-phase optimization of the bare QM0 region leads to much less twisted structures in all cases, as expected (see entry 2 in Table 5). The twist of the retinal backbone is already largely restored in QM/MM optimizations that include only the electrostatic interactions between QM0 and Glu113 (see entry 3 in Table 5). Finally, when turning off these electrostatic interactions with Glu113 in the QM/MM optimizations, the twist becomes notably larger in hWT but changes less in the two mutants (see entries 1 and 4 in Table 5).

Table 6. Bond Length Alternation (Å) in the Human Wild-Type Rhodopsin and the Mutants for the Standard QM/MM Setup (Model I, ref) and for the Model Systems 1−4 (See Text)[a]

	hWT	hM207R	hS186W
ref	0.43	0.50	0.56
1	0.39	0.49	0.54
2	0.22	n/a	0.55
3	0.44	0.44	0.57
4	0.23	0.37	0.57

[a] See footnote [a] of Table 5.

As already discussed, the bond length alternation in the retinal chain increases for our standard QM/MM setup when going from hWT to hM207R and hS186W (Table 6). The BLA values change only slightly when using the smaller QM0 region (see entry 1 in Table 6). In the case of hWT and hM207R, they remain large when including only the electrostatic QM/MM interactions with the anionic Glu113 residue (see entry 3 in Table 5) but become much smaller in the gas-phase model calculations where this residue is not present (see entry 2 in Table 6) and in the QM/MM calculations when turning off the MM charges of Glu113 (see entry 4 in Table 6). By contrast, in the case of the hS186W mutant with a neutral Glu113 residue, the BLA values remain essentially the same in all model systems (Table 6).

The DFT/MRCI vertical excitation energies for our standard QM/MM setup give a strong blue shift of the first bright transition in the mutants, both in hM207R and even more so in hS186W (Table 7). The computed QM/MM values change only slightly when using the smaller QM0 region (see entry 1 of Table 7). Since hWT and hM207R share the same bare QM0 region, the corresponding excitation energies must be identical (not computed for hM207R); the calculated value for hWT is much smaller than in the protein (see entry 2 in Table 7) but increases substantially when adding an anionic Glu113 residue (see entry 3 in Table 7). The absence or presence of Glu113 thus strongly affects the vertical excitation energies of hWT and hM207R (see also entries 1 and 4 in Table 7). In the hS186W mutant, the gas-phase excitation energy of the bare QM0 region (retinal plus unprotonated Lys296) is computed to be very high (see entry 2 in Table 7), and is reduced only slightly upon

Table 7. DFT/MRCI Vertical Excitation Energies of the First Bright Transition *E* (eV) and Oscillator Strengths *f* in the Human Wild-Type Rhodopsin and the Mutants for the Standard QM/MM Setup (Model I, ref) and for the Model Systems 1−4 (See Text), Evaluated at the Individually Optimized Structures[a,b]

	hWT		hM207R		hS186W	
	E	*f*	*E*	*f*	*E*	*f*
ref	2.50	1.26	2.93	1.22	3.05	1.07
1	2.39	1.26	2.87	1.24	3.06	1.12
2	1.99	1.54	n/a	n/a	3.48	1.22
3	2.61	1.26	2.58	1.27	3.30	0.95
4	1.94	1.42	2.27	1.35	3.10	1.02

[a] See footnote [a] of Table 5. [b] The data in this table refer to the brightest low-energy transition that is dominated by the $\pi\pi^*$ HOMO−LUMO excitation. This transition generates the S_1 state in all cases except for entry 2 of hS186W (neutral gas-phase chromophore) where the HOMO−LUMO excitation contributes to the three lowest singlet excited states as follows: S_1 at 3.25 eV, 38%; S_2 at 3.26 eV, 21%; S_3 at 3.48 eV, 55%.

addition of a neutral Glu113 residue (see entry 3 in Table 7); the minor role of this neutral residue in hS186W is also obvious from the QM/MM charge deletion analysis (see entries 1 and 4 in Table 7). The DFT/MRCI vertical excitation energies calculated at individually optimized geometries (Table 7) do not change much when reevaluating all of them at the optimized geometries obtained from our standard QM/MM setup (see Table S7, Supporting Information), and hence, the trends discussed above remain valid for this alternative choice of geometries.

The results in Tables 5−7 indicate that the spectral tuning follows different mechanisms in the three proteins considered presently. In hWT and hM207MR, the anionic Glu113 residue has a strong direct influence on the excitation energy, but the main distinguishing feature is the structure of the retinal chain, which shows a higher twist and a larger bond length alternation in the full and approximate QM/MM treatments (Tables 5 and 6). In the hS186W mutant, the intrinsic excitation energy of the isolated chromophore (with a neutral deprotonated Lys296 residue) is already much higher and accounts for the basic blue shift in the protein; the retinal chain is strongly twisted and has a very pronounced bond length alternation at all levels considered, while the neutral Glu113 residue has only a minor influence (Tables 5 and 6). This strong intrinsic blue shift of the neutral chromophore is well-known experimentally: gas-phase absorption spectra of neutral retinal Schiff base chromophores show blue shifts up to 1.17 eV compared with their protonated counterparts.[113] On the theoretical side, high-level ab initio (CASPT2) calculations give a blue shift of 1.40 eV upon deprotonation of the Schiff base chromophore,[114] in good agreement with the present results (Table 7). Qualitatively, this intrinsic shift is caused by the charge transfer that occurs upon HOMO−LUMO excitation from the ionone side toward the SBL side (see Figure 12), which is energetically much favored when Lys296 is protonated.[113]

To summarize, in agreement with other studies on bovine and squid rhodopsins,[12,67,110] the spectral tuning in hM207R is mainly due to the Glu113 counterion and the structural features of the retinal chain, whereas the presence of neutral Lys296 and Glu113 residues is mainly responsible for the strong blue shift in the hS186W mutant.

Excess Energy in Mutants. The hM207R and hS186W mutations lead to a substantial increase of the first vertical excitation energy compared with the native human rhodopsin (hWT). The calculated vertical excitation energy of hWT (57.7 kcal/mol) matches the reported experimental value well (57.4 kcal/mol).[103] The excitation energy is computed to be higher by 9.9 kcal/mol in the hM207R mutant and by 12.7 kcal/mol in the hS186W mutant. One may thus hypothesize that this higher energy uptake could be related to the pathogeny of the *Retinitis pigmentosa* disease at a molecular level, since it can cause harmful collateral reactions in the retinal binding site of the mutated systems.

Experimentally, the energy for rhodopsin activation by light in vertebrate rods is on the order of 40−50 kcal/mol,[115] and after the photoinduced 11-*cis*/all-*trans* isomerization, an energy amount of about 32−35 kcal/mol is stored in the bathorhodopsin intermediate.[103] In hWT, the difference between the energy absorbed by rhodopsin and stored in bathorhodopsin (i.e., the excess energy) is thus around 22−25 kcal/mol. Assuming that the bathorhodopsin intermediate has a similar endothermicity in the wild type and the mutants, the excess energy is predicted to be in the range 32−38 kcal/mol in hM207R and hS186W. We note in this context a recent QM/MM study of vertebrate (bovine) and invertebrate (squid) rhodopsins,[116] which addressed energy storage in the corresponding bathorhodopsin intermediates and its relation to the flexibility of the binding site.

CONCLUSIONS

The geometries, electronic structures, and vertical excitation energies of two human rhodopsin mutants (hM207R and hS186W) associated with the *Retinitis pigmentosa* disease were investigated using MD simulations as well as QM/MM and DFT/MRCI calculations. An analogous study of the wild-type bovine and human rhodopsins was carried out for comparison, yielding results that are in good agreement with previous experimental and theoretical work on these wild-type proteins. An analysis of the QM energies shows that the chromophore−counterion region is less stable in the mutants compared to the wild type, consistent with recent protein folding studies that indicate some destabilization of the whole protein due to mutation.[23] The present calculations provide insight into the spectral shifts in the mutants and their relation to structural and electronic effects.

We find that both mutations lead to slightly less twisted dark state configurations and to a strong blue shift of the vertical excitation energies. The excess energy found in the mutants (compared with the wild-type rhodopsins) could lead to unwanted side reactions in the absence of a sufficiently fast energy dissipation mechanism.

As in previous work, a positive correlation is observed between the computed BLA values and vertical excitation energies. The higher S_1 vertical excitation energies in the mutants are consistent with the calculated BLA values and the electronic structure of both mutants. The electronic polarization effects of Arg207 and the electrostatic influence from the counterion Glu113 explain the higher vertical excitation energy of the hM207R mutant. The chromophore in hS186W contains a neutral Schiff base linkage which is known to show a substantial blue shift of the lowest excitation (compared with its protonated counterpart), and there is an increased electronic polarization of the β-ionone

ring, which leads to the highest BLA values, the best localized HOMO (in the ring), and the highest vertical excitation energy found presently. The spectral tuning is thus mainly associated with counterion effects and structural features of the retinal chain in the case of the hM207R mutant, and with the presence of a neutral chromophore containing deprotonated Lys296 in the case of the hS186W mutant.

■ ASSOCIATED CONTENT

Supporting Information. Structural validation of the homology models, NBO charges, pK_a values, and other tables and figures. This material is available free of charge via the Internet at http://pubs.acs.org.

■ AUTHOR INFORMATION

Corresponding Author
*E-mail: esanchez@mpi-muelheim.mpg.de.

■ ACKNOWLEDGMENT

E.W.H.-R. thanks Sandra M. Blois for supporting this work within the framework of the cooperation between the Charité-Universitätsmedizin Berlin and the Havana Higher Institute of Medical Sciences in Cuba as well as Elke Gnielka. E.W.H.-R. acknowledges Alejandro Gil and Reynier Suardiaz for useful suggestions. E.W.H.-R. and E.S.-G. thank Oliver Weingart, Mario da Silva Junior, Iakov Polyak, and Markus Doerr from the Max-Planck-Institut für Kohlenforschung for fruitful discussions. E.S.-G. thanks the Funds of the German Chemical Industry for financial support. The Charité-Universitätsmedizin Berlin and the Max-Planck-Institut für Kohlenforschung were the host institutions for this work. The Autonomous University of Madrid provided part of the computational facilities.

■ REFERENCES

(1) Merin, S.; Auerbach, E. *Surv. Ophthalmol.* **1976**, *20*, 303–346.
(2) Baumgartner, W. A. *Med. Hypotheses* **2000**, *54*, 814–824.
(3) Mendes, H. F.; Van Der Spuy, J.; Chapple, J. P.; Cheetham, M. E. *Trends Mol. Med.* **2005**, *11*, 177–185.
(4) Palczewski, K. *Annu. Rev. Biochem.* **2006**, *75*, 743–767.
(5) Ernst, O. P.; Gramse, V.; Kolbe, M.; Hofmann, K. P.; Heck, M. *Proc. Natl. Acad. Sci. U.S.A.* **2007**, *104*, 10859–10864.
(6) Menon, S. T.; Han, M.; Sakmar, T. P. *Physiol. Rev.* **2001**, *81* 1659–1688.
(7) Hubbard, R. *Nature* **1969**, *221*, 432–435.
(8) Bravaya, K.; Bochenkova, A.; Granovsky, A.; Nemukhin, A. *J. Am. Chem. Soc.* **2007**, *129*, 13035–13042.
(9) Röhrig, U. F.; Guidoni, L.; Rothlisberger, U. *Biochemistry* **2002**, *41*, 10799–10809.
(10) Okada, T.; Ernst, O. P.; Palczewski, K.; Hofmann, K. P. *Trends Biochem. Sci.* **2001**, *26*, 318–324.
(11) McBee, J. K.; Palczewski, K.; Bähr, W.; Pepperberg, D. R. *Prog. Retinal Eye Res.* **2001**, *20*, 469–529.
(12) Altun, A.; Yokoyama, S.; Morokuma, K. *J. Phys. Chem. B* **2008**, *112*, 6814–6827.
(13) Altun, A.; Yokoyama, S.; Morokuma, K. *Photochem. Photobiol.* **2008**, *84*, 845–854.
(14) Okada, T.; Sugihara, M.; Bondar, A.-N.; Elstner, M.; Entel, P.; Buss, V. *J. Mol. Biol.* **2004**, *342*, 571–583.
(15) Tsutsui, K.; Shichida, Y. *Photochem. Photobiol. Sci.* **2010**, *9*, 1426–1434.
(16) Tsutsui, K.; Imai, H.; Shichida, Y. *Biochemistry* **2007**, *46*, 6437–6445.
(17) Weingart, O.; Altoe, P.; Stenta, M.; Bottoni, A.; Orlandi, G.; Garavelli, M. *Phys. Chem. Chem. Phys.* **2011**, *13*, 3645–3648.
(18) Buss, V.; Weingart, O.; Sugihara, M. *Angew. Chem., Int. Ed.* **2000**, *39*, 2784–2786.
(19) Weingart, O. *J. Am. Chem. Soc.* **2007**, *129*, 10618–10619.
(20) Garriga, P.; Liu, X.; Khorana, H. G. *Proc. Natl. Acad. Sci. U.S.A.* **1996**, *93*, 4560–4564.
(21) Liu, X.; Garriga, P.; Khorana, H. G. *Proc. Natl. Acad. Sci. U.S.A.* **1996**, *93*, 4554–4559.
(22) Andres, A.; Garriga, P.; Manyosa, J. *Biochem. Biophys. Res. Commun.* **2003**, *303*, 294–301.
(23) Rakoczy, E. P.; Kiel, C.; McKeone, R.; Stricher, F.; Serrano, L. *J. Mol. Biol.* **2011**, *405*, 584–606.
(24) Stojanovic, A.; Hwa, J. *Recept. Channels* **2002**, *8*, 33–50.
(25) Burns, M. E.; Arshavsky, V. Y. *Neuron* **2005**, *48*, 387–401.
(26) Chuang, J.-Z.; Vega, C.; Jun, W.; Sung, C.-H. *J. Clin. Invest.* **2004**, *114*, 131–140.
(27) Kennan, A.; Aherne, A.; Humphries, P. *Trends Genet.* **2005**, *21*, 103–110.
(28) Del Valle, L. J.; Ramon, E.; Bosch, L.; Manyosa, J.; Garriga, P. *Cell. Mol. Life Sci.* **2003**, *60*, 2532–2537.
(29) Kaushal, S.; Khorana, H. G. *Biochemistry* **1994**, *33*, 6121–6128.
(30) Janz, J. M.; Fay, J. F.; Farrens, D. L. *J. Biol. Chem.* **2003**, *278*, 16982–16991.
(31) Ridge, K. D.; Ngo, T.; Lee, S. S. J.; Abdulaev, N. G. *J. Biol. Chem.* **1999**, *274*, 21437–21442.
(32) Breikers, G.; Portier-VandeLuytgaarden, M. J. M.; Bovee-Geurts, P. H. M.; DeGrip, W. J. *Biochem. Biophys. Res. Commun.* **2002**, *297*, 847–853.
(33) Hwa, J.; Garriga, P.; Liu, X.; Khorana, H. G. *Proc. Natl. Acad. Sci. U.S.A.* **1997**, *94*, 10571–10576.
(34) Jäger, S.; Han, M.; Lewis, J. W.; Szundi, I.; Sakmar, T. P.; Kliger, D. S. *Biochemistry* **1997**, *36*, 11804–11810.
(35) Aguila, M.; Toledo, D.; Morillo, M.; Dominguez, M.; Vaz, B.; Alvarez, R.; de Lera, A. R.; Garriga, P. *Photochem. Photobiol.* **2009**, *85*, 485–493.
(36) Felline, A.; Seeber, M.; Rao, F.; Fanelli, F. *J. Chem. Theory Comput.* **2009**, *5*, 2472–2485.
(37) Liu, M. Y.; Liu, J.; Yan, E. C. Y. *Abstracts, 36th Northeast Regional Meeting of the American Chemical Society, Hartford, CT, United States* 2009, NERM-326.
(38) Padron-Garcia, J. A.; Crespo-Otero, R.; Hernandez-Rodriguez, E. W.; Garriga, P.; Montero, L. A.; Garcia-Pineiro, J. C. *Proteins: Struct., Funct., Bioinf.* **2004**, *57*, 392–399.
(39) Blatz, P. E.; Liebman, P. A. *Exp. Eye Res.* **1973**, *17*, 573–580.
(40) Kakitani, H.; Kakitani, T.; Rodman, H.; Honig, B. *Photochem. Photobiol.* **1985**, *41*, 471–479.
(41) Kropf, A.; Hubbard, R. *Ann. N. Y. Acad. Sci.* **1958**, *74*, 266–280.
(42) Neitz, M.; Neitz, J.; Jacobs, G. H. *Science* **1991**, *252*, 971–974.
(43) Beppu, Y.; Kakitani, T. *Photochem. Photobiol.* **1994**, *59*, 660–669.
(44) Honig, B.; Greenberg, A. D.; Dinur, U.; Ebrey, T. G. *Biochemistry* **1976**, *15*, 4593–4599.
(45) Baasov, T.; Friedman, N.; Sheves, M. *Biochemistry* **1987**, *26*, 3210–3217.
(46) Rodriguez, R.; Chinea, G.; Lopez, N.; Pons, T.; Vriend, G. *Bioinformatics* **1998**, *14*, 523–528.
(47) van der Kamp, M. W.; Shaw, K. E.; Woods, C. J.; Mulholland, A. J. *J. R. Soc. Interface* **2008**, *5*, S173–S190.
(48) Senn, H. M.; Thiel, W. *Angew. Chem., Int. Ed.* **2009**, *48*, 1198–1229.
(49) Grimme, S.; Waletzke, M. *J. Chem. Phys.* **1999**, *111*, 5645–5655.
(50) Bauernschmitt, R.; Häser, M.; Treutler, O.; Ahlrichs, R. *Chem. Phys. Lett.* **1997**, *264*, 573–578.
(51) van Gisbergen, S. J. A. S., J.; Baerends, E. J. *J. Chem. Phys.* **1995**, *103*, 9347–9354.

(52) Jamorski, C. C., M. E.; Salahub, D. R. *J. Chem. Phys.* **1996**, *104*, 5134–5147.
(53) Petersilka, M. G., U. J.; Gross, E. K. U. *Phys. Rev. Lett.* **1996**, *76*, 1212–1215.
(54) Protein Data Bank. www.pdb.org (accessed Sept 1, 2009).
(55) Altschul, S. F.; Boguski, M. S.; Gish, W.; C., W. J. *Nat. Genet.* **1994**, *6*, 119–129.
(56) ExPASy Molecular Biology Server. http://www.mrc-lmb.cam.ac.uk/genomes/madanm/pres/swiss1.htm (accessed October 20, 2009).
(57) Sali, A.; Blundell, T. L. *J. Mol. Biol.* **1993**, *234*, 779–815.
(58) Sali, A.; Potterton, L.; Yuan, F.; van Vlijmen, H.; Karplus, M. *Proteins: Struct., Funct., Genet.* **1995**, *23*, 318–326.
(59) Li, H.; Robertson, A. D.; Jensen, J. H. *Proteins: Struct., Funct., Bioinf.* **2005**, *61*, 704–721.
(60) Chen, C.; Jiang, Y.; Koutalos, Y. *Biophys. J.* **2002**, *83*, 1403–1412.
(61) Fahmy, K.; Jager, F.; Beck, M.; Zvyaga, T. A.; Sakmar, T. P.; Siebert, F. *Proc. Natl. Acad. Sci. U.S.A.* **1993**, *90*, 10206–10210.
(62) Yan, E. C. Y.; Kazmi, M. A.; De, S.; Chang, B. S. W.; Seibert, C.; Marin, E. P.; Mathies, R. A.; Sakmar, T. P. *Biochemistry* **2002**, *41*, 3620–3627.
(63) Mollevanger, L. C. P. J; Kentgens, A. P. M; Pardoen, J. A.; Courtin, J. M. L.; Veeman, W. S.; Lugtenburg, J.; De Grip, W. J. *Eur. J. Biochem.* **1987**, *163*, 9–14.
(64) Han, M.; Smith, S. O. *Biochemistry* **1995**, *34*, 1425–1432.
(65) Frähmcke, J. S.; Wanko, M.; Phatak, P.; Mroginski, M. A.; Elstner, M. *J. Phys. Chem. B* **2010**, *114*, 11338–11352.
(66) Birge, R. R.; Murray, L. P.; Pierce, B. M.; Akita, H.; Balogh-Nair, V.; Findsen, L. A.; Nakanishi, K. *Proc. Natl. Acad. Sci. U.S.A.* **1985**, *82*, 4117–4121.
(67) Sekharan, S.; Buss, V. *J. Am. Chem. Soc.* **2008**, *130*, 17220–17221.
(68) Cai, K.; Klein-Seetharaman, J.; Farrens, D.; Zhang, C.; Altenbach, C.; Hubbell, W. L.; Khorana, H. G. *Biochemistry* **1999**, *38*, 7925–7930.
(69) Phillips, J. C.; Braun, R.; Wang, W.; Gumbart, J.; Tajkhorshid, E.; Villa, E.; Chipot, C.; Skeel, R. D.; Kale, L.; Schulten, K. *J. Comput. Chem.* **2005**, *26*, 1781–1802.
(70) Bowie, J. U.; Luthy, R.; Eisenberg, D. *Science* **1991**, *253*, 164–170.
(71) Laskowski, R. A.; MacArthur, M. W.; Moss, D. S.; Thornton, J. M. *J. Appl. Crystallogr.* **1993**, *26*, 283–291.
(72) Hooft, R. W. W.; Vriend, G.; Sander, C.; Abola, E. E. *Nature (London)* **1996**, *381*, 272.
(73) Fong, S. L.; Tsin, A. T. C.; Bridges, C. D. B.; Liou, G. I. *Methods Enzymol.* **1982**, *81*, 133–140.
(74) Saam, J.; Tajkhorshid, E.; Hayashi, S.; Schulten, K. *Biophys. J.* **2002**, *83*, 3097–3112.
(75) Humphrey, W.; Dalke, A.; Schulten, K. *J. Mol. Graphics* **1996**, *14*, 33–38.
(76) Grubmüller, H.; Groll, V. Solvate 1.0; University of Munich, see http://www.mpibpc.mpg.de/home/grubmueller/downloads/solvate/index.html (accessed October 11, 2010).
(77) Brooks, B. R.; Bruccoleri, R. E.; Olafson, B. D.; States, D. J.; Swaminathan, S.; Karplus, M. J. *J. Comput. Chem.* **1983**, *4*, 187–217.
(78) MacKerell, A. D.; Brooks, B.; Brooks, C. L., III; Nilsson, L.; Roux, B.; Won, Y.; Karplus, M. In *The Encyclopedia of Computational Chemistry*; Schleyer, P. v. R., Allinger, N. L., Clark, T., Gasteiger, J., Kollman, P., Schaefer, H. F., III, Eds.; John Wiley & Sons: Chichester, U.K., 1998; pp 271−277.
(79) Nina, M.; Roux, B.; Smith, J. C. *Biophys. J.* **1995**, *68*, 25–39.
(80) Ryckaert, J.-P.; Ciccotti, G.; Berendsen, H. J. C. *J. Comput. Phys.* **1977**, *23*, 327–341.
(81) MacKerell, A. D., Jr.; Bashford, D.; Bellott, M.; Dunbrack, R. L.; Evanseck, J. D.; Field, M. J.; Fischer, S.; Gao, J.; Guo, H.; Ha, S. *J. Phys. Chem. B* **1998**, *102*, 3586–3616.
(82) MacKerell, A. D., Jr.; Feig, M.; Brooks, C. L., III. *J. Comput. Chem.* **2004**, *25*, 1400–1415.
(83) Jorgensen, W. L.; Chandrasekhar, J.; Madura, J. D. *J. Chem. Phys.* **1983**, *79*, 926–928.
(84) Essmann, U.; Perera, L.; Berkowitz, M. L.; Darden, T.; Lee, H.; Pedersen, L. G. *J. Chem. Phys.* **1995**, *103*, 8577–8593.
(85) Babitzki, G.; Denschlag, R.; Tavan, P. *J. Phys. Chem. B* **2009**, *113*, 10483–10495.
(86) Sherwood, P.; de Vries, A. H.; Guest, M. F.; Schreckenbach, G.; Catlow, C. R. A.; French, S. A.; Sokol, A. A.; Bromley, S. T.; Thiel, W.; Turner, A. J. *THEOCHEM* **2003**, *632*, 1–28.
(87) Ahlrichs, R.; Bär, M.; Häser, M.; Horn, H.; Kölmel, C. *Chem. Phys. Lett.* **1989**, *162*, 165–169.
(88) Smith, W.; Forester, T. R. *J. Mol. Graphics* **1996**, *14*, 136–141.
(89) Dirac, P. A. M. *Proc. R. Soc. London, Ser. A* **1929**, *123*, 714–733.
(90) Slater, J. C. *Phys. Rev. A* **1951**, *81*, 385–390.
(91) Becke, A. D. *J. Chem. Phys.* **1993**, *98*, 5648–5652.
(92) Becke, A. D. *Phys. Rev. A* **1988**, *38*, 3098–3100.
(93) Lee, C.; Yang, W.; Parr, R. G. *Phys. Rev. B* **1988**, *37*, 785–789.
(94) Bakowies, D.; Thiel, W. *J. Phys. Chem.* **1996**, *100*, 10580–10594.
(95) de Vries, A. H.; Sherwood, P.; Collins, S. J.; Rigby, A. M.; Rigutto, M.; Kramer, G. J. *J. Phys. Chem. B* **1999**, *103*, 6133–6141.
(96) Antes, I.; Thiel, W. *ACS Symp. Ser.* **1998**, *712*, 50–65.
(97) Billeter, S. R.; Turner, A. J.; Thiel, W. *Phys. Chem. Chem. Phys.* **2000**, *2*, 2177–2186.
(98) Levine, B. G.; Ko, C.; Quenneville, J.; Martinez, T. J. *Mol. Phys.* **2006**, *104*, 1039–1051.
(99) Becke, A. D. *J. Chem. Phys.* **1993**, *98*, 1372–1377.
(100) Gerenkamp, M. Ph.D. Thesis, Universität Münster, 2005.
(101) Silva-Junior, M. R.; Schreiber, M.; Sauer, S. P. A; Thiel, W. *J. Chem. Phys.* **2008**, *129*, 104103.
(102) Huber, T.; Botelho, A. V.; Beyer, K.; Brown, M. F. *Biophys. J.* **2004**, *86*, 2078–2100.
(103) Gascon, J. A.; Batista, V. S. *Biophys. J.* **2004**, *87*, 2931–2941.
(104) Röhrig, U. F.; Guidoni, L.; Rothlisberger, U. *ChemPhysChem* **2005**, *6*, 1836–1847.
(105) Sekharan, S.; Altun, A.; Morokuma, K. *Chem.—Eur. J.* **2010**, *16*, 1744–1749.
(106) Röhrig, U. F.; Guidoni, L.; Laio, A.; Frank, I.; Rothlisberger, U. *J. Am. Chem. Soc.* **2004**, *126*, 15328–15329.
(107) Sekharan, S.; Altun, A.; Morokuma, K. *J. Am. Chem. Soc.* **2010**, *132*, 15856–15859.
(108) Wanko, M.; Hoffmann, M.; Strodel, P.; Koslowski, A.; Thiel, W.; Neese, F.; Frauenheim, T.; Elstner, M. *J. Phys. Chem. B* **2005**, *109*, 3606–3615.
(109) Hufen, J.; Sugihara, M.; Buss, V. *J. Phys. Chem. B* **2004**, *108*, 20419–20426.
(110) Sekharan, S.; Sugihara, M.; Buss, V. *Angew. Chem., Int. Ed.* **2007**, *46*, 269–271.
(111) Hoffmann, M.; Wanko, M.; Strodel, P.; Koenig, P. H.; Frauenheim, T.; Schulten, K.; Thiel, W.; Tajkhorshid, E.; Elstner, M. *J. Am. Chem. Soc.* **2006**, *128*, 10808–10818.
(112) Tavan, P.; Schulten, K. *J. Chem. Phys.* **1986**, *85*, 6602–6609.
(113) Nielsen, I. B.; Petersen, M. Å.; Lammich, L.; Nielsen, M. B.; Andersen, L. H. *J. Phys. Chem. A* **2006**, *110*, 12592–12596.
(114) Sekharan, S.; Weingart, O.; Buss, V. *Biophys. J.* **2006**, L07–L09.
(115) Ala-Laurila, P.; Donner, K.; Koskelainen, A. *Biophys. J.* **2004**, *86*, 3653–3662.
(116) Sekharan, S.; Morokuma, K. *J. Am. Chem. Soc.* **2011**, *133*, 4734–4737.